HHS Public Access

Author manuscript

Cell Rep. Author manuscript; available in PMC 2021 March 17.

Published in final edited form as:

Cell Rep. 2021 February 09; 34(6): 108729. doi:10.1016/j.celrep.2021.108729.

Prenatal correction of IGF2 to rescue the growth phenotypes in mouse models of Beckwith-Wiedemann and Silver-Russell syndromes

Ji Liao[1], **Tie-Bo Zeng**[1], **Nicholas Pierce**[1], **Diana A. Tran**[2,3], **Purnima Singh**[2,5], **Jeffrey R. Mann**[2,4], **Piroska E. Szabó**[1,6,*]

[1]Center for Epigenetics, Van Andel Institute, Grand Rapids, MI 49503, USA

[2]Division of Molecular and Cellular Biology, City of Hope Cancer Center, Duarte, CA 91010, USA

[3]Irell and Manella Graduate School, City of Hope, Duarte, CA 91010, USA

[4]Present address: Biomedicine Discovery Institute, Monash University Clayton Campus, VIC 3800, Australia

[5]Present address: Institute for Cancer Outcomes and Survivorship, University of Alabama at Birmingham, Birmingham, AL, USA

[6]Lead contact

SUMMARY

Beckwith-Wiedemann syndrome (BWS) and Silver-Russell syndrome (SRS) are imprinting disorders manifesting as aberrant fetal growth and severe postnatal-growth-related complications. Based on the insulator model, one-third of BWS cases and two-thirds of SRS cases are consistent with misexpression of insulin-like growth factor 2 (IGF2), an important facilitator of fetal growth. We propose that the IGF2-dependent BWS and SRS cases can be identified by prenatal diagnosis and can be prevented by prenatal intervention targeting IGF2. We test this hypothesis using our mouse models of IGF2-dependent BWS and SRS. We find that genetically normalizing IGF2 levels in a double rescue experiment corrects the fetal overgrowth phenotype in the BWS model and the growth retardation in the SRS model. In addition, we pharmacologically rescue the BWS growth phenotype by reducing IGF2 signaling during late gestation. This animal study encourages clinical investigations to target IGF2 for prenatal diagnosis and prenatal prevention in human BWS and SRS.

*Correspondence: piroska.szabo@vai.org.

AUTHOR CONTRIBUTIONS

Conceptualization, P.E.S. and J.R.M.; formal analysis, N.P.; funding acquisition, P.E.S.; investigation, J.L., T.-B.Z., N.P., D.A.T., P.S., and P.E.S.; methodology, P.E.S. and J.R.M.; supervision, P.E.S.; validation, J.L., T.-B.Z., N.P., and P.E.S.; visualization, N.P. and P.E.S.; writing – original draft, P.E.S.; writing – review & editing, J.L., T.-B.Z., N.P., D.A.T., P.S., P.E.S., and J.R.M.

SUPPLEMENTAL INFORMATION

Supplemental information can be found online at https://doi.org/10.1016/j.celrep.2021.108729.

DECLARATION OF INTERESTS

The authors declare no competing interests.

Graphical Abstract

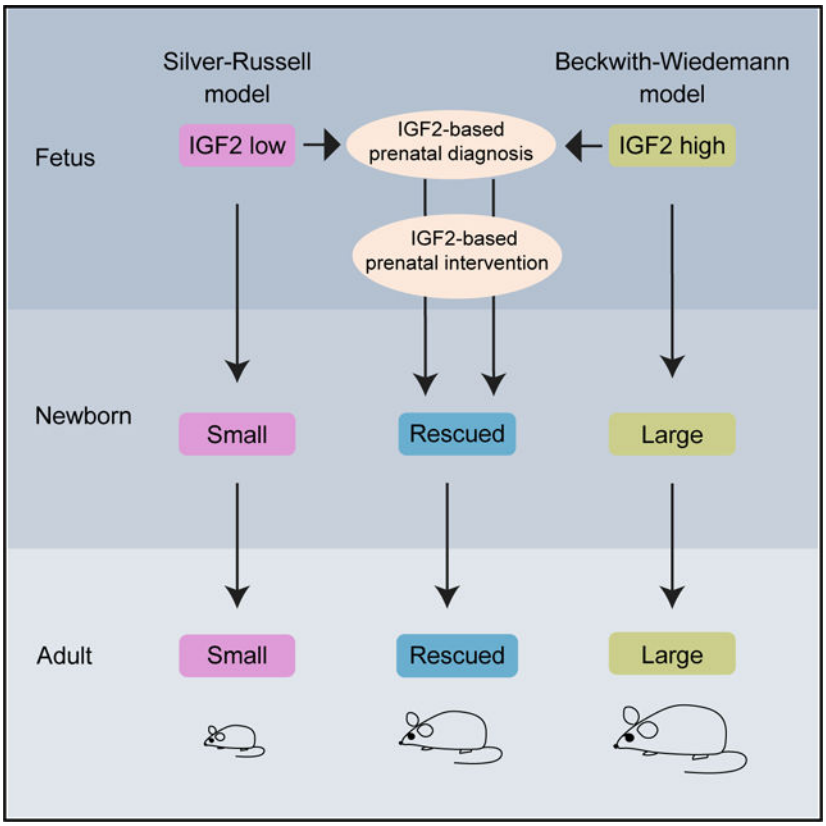

In Brief

Liao et al. use mouse models to test a prenatal approach for correcting growth anomalies in two imprinting diseases, BWS and SRS. They find that cases where the fetal growth factor IGF2 is misregulated can be diagnosed, and growth can be corrected by prenatally adjusting IGF2 or its signaling output.

INTRODUCTION

Beckwith-Wiedemann syndrome (BWS; OMIM 130650) and Silver-Russell syndrome (SRS; OMIM 180860) are imprinting disorders (Monk et al., 2019) that display fetal overgrowth and fetal growth retardation, respectively. Most BWS symptoms (Brioude et al., 2018) directly or indirectly depend on aberrant growth regulation during gestation: large birth weight; enlarged placenta, tongue, kidney, and liver; and childhood cancers associated with overgrowth (Brioude et al., 2019), such as Wilms tumor of the kidney. A total of 68% of BWS children undergo at least one surgery related to BWS, including tongue or kidney reduction or cancer treatment (McNeil et al., 2002; Naujokat et al., 2019; Style et al., 2018). SRS symptoms (Wakeling et al., 2017) that depend on aberrant growth regulation include small for gestational age (SGA), relative macrocephaly at birth, severe feeding difficulties, and low body mass index.

The opposite growth anomalies of BWS and SRS correspond to the reciprocal genetic and epigenetic (DNA methylation) defects of the same genetic region (Eggermann, 2009). Approximately 80% of BWS and 60% of SRS cases have a molecular defect at chromosome 11p15.5 (Kalish et al., 2014) that hosts two imprinted domains. In domain 1, the paternally expressed *insulin-like growth factor 2* (*IGF2*) gene, regulated by the imprinting control region 1 (ICR1), promotes growth, and in domain 2, the maternally expressed *cyclin-dependent kinase inhibitor 1c* (*CDKN1C*), regulated by the imprinting control region 2 (ICR2), inhibits growth. The phenotypes of BWS and SRS can be effectively modeled in the mouse (Chang and Bartolomei, 2020). *Cdkn1c* mutant mice do not exhibit neonatal overgrowth (Tunster et al., 2011), whereas models with *Igf2* misregulation manifest in fetal and neonatal BWS-like overgrowth or SRS-like growth retardation (Singh et al., 2012).

IGF2 encodes the fetal growth factor IGF2. Its RNA is expressed in the chromosome inherited from the father in mice and humans (DeChiara et al., 1991; Giannoukakis et al., 1993). Our knowledge regarding mechanisms that regulate the paternal allele-specific expression of *IGF2* is based on genetic studies that focused on the orthologous mouse *Igf2-H19* imprinted domain, as summarized in Figure 1A (Singh et al., 2012). IGF2 regulates the supply of nutrients by the placenta and also the demand for nutrients by the fetus (Constância et al., 2002). *H19* is a non-coding RNA expressed from the maternally inherited chromosome (Bartolomei et al., 1991; Ferguson-Smith et al., 1993). The *H19* RNA releases miR-675 at late gestation to suppress the growth of the placenta just before birth (Keniry et al., 2012). *Igf2* and *H19* are co-regulated in organs of endoderm and mesoderm origin by their shared enhancers (Leighton et al., 1995b). The genomic imprint of this domain is inherited from the father and consists of CpG methylation along the ICR1 (Thorvaldsen et al., 1998). In the soma, ICR1 functions as a DNA-methylation-sensitive insulator (Figure 1A). We and others reported that four CTCF molecules bind in the unmethylated maternal ICR1 allele to insulate the *Igf2* gene from its enhancers, but in the paternal allele, CTCF binding is prevented by DNA methylation, allowing *Igf2* transcription (Bell and Felsenfeld, 2000; Hark et al., 2000; Kaffer et al., 2000; Kanduri et al., 2000; Szabó et al., 2000).

BWS molecular defects at the ICR1 can be genetic or epigenetic (Brioude et al., 2018). The insulator model (Figure 1A) predicts that in each of these BWS classes (Figures S1A–S1C; Azzi et al., 2014; Bachmann et al., 2017; Brioude et al., 2018; Netchine et al., 2013; Riccio et al., 2009) *IGF2* is transcribed from two chromosomes instead of one, resulting in an elevated dose of IGF2 protein, which causes the overgrowth symptoms. In mouse genetic models, an increased dose of *Igf2* recapitulated the overgrowth phenotypes of BWS. These models include the *Igf2* transgenic mice (Eggenschwiler et al., 1997; Sun et al., 1997), mice with paternal duplication of distal chromosome 7 (PatDup.dist7) (Rentsendorj et al., 2010), and mice that carry mutation in the CTCF binding sites in the maternal ICR1 allele (Szabó et al., 2004). Elevated and biallelic *IGF2* RNA expression was found in the tongue and fibroblast of human BWS patients (Weksberg et al., 1993; Reik et al., 1995), supporting the insulator model in humans.

The complex genetic and epigenetic molecular defects found in SRS at the ICR1 (Figures S1D and S1E; Azzi et al., 2014; Begemann et al., 2015; Eggermann et al., 2006; Gicquel et al., 2005; Peñaherrera et al., 2010; Wakeling et al., 2017; Liu et al., 2017; Yamoto et al.,

2017) are consistent with reduced *IGF2* expression and fetal growth retardation. Mice that carry an *Igf2* null mutation are 60% the size of normal siblings (DeChiara et al., 1990). Very small size also characterizes the embryos carrying maternal duplication of distal chromosome 7 MatDup.dist7 (Han et al., 2010) and fetuses that are engineered to exhibit biallelic ICR1 insulation (Lee et al., 2010; Szabó et al., 2002; Engel et al., 2004), due to greatly reduced *Igf2* levels. Reduced *IGF2* RNA levels in human SRS fibroblasts (Gicquel et al., 2005) and epimutation positive fetuses and placentas (Yamazawa et al., 2008) support the insulator model in humans. Reduced IGF2 protein levels in SRS children (Begemann et al., 2015; Binder et al., 2017) suggest the involvement of IGF2 misregulation in SRS.

The goal of the current work was to address three clinical challenges: (1) IGF2, a known facilitator of fetal growth, has not been targeted in clinical therapy of BWS or SRS; (2) BWS and SRS children are normally diagnosed after birth, when most of the symptoms have already developed and IGF2 levels can no longer be corrected efficiently; and (3) the management of these diseases does not include prenatal intervention. To address these challenges, we used mouse models to derive proof-of principle evidence showing that IGF2-based diagnosis and therapy at the fetal stage could prevent the overgrowth symptoms of BWS and the growth retardation of SRS.

RESULTS

Animal models of BWS and SRS

We previously generated gene-targeted mouse lines to model the molecular features of BWS and SRS cases that are related to the ICR1 (Lee et al., 2010; Szabó et al., 2002, 2004). The BWS model (CTCFm/+, the mother's genotype is always written first) was created by introducing point mutations in the four CTCF binding sites (CTCFm allele) in the maternal ICR1 allele (Szabó et al., 2004). *Igf2* is biallelically expressed in the absence of enhancer insulation (Figure 1B), resulting in fetal overgrowth. The SRS model (+/CHB) (Lee et al., 2010) was generated by replacing the methylated, paternal *H19* ICR1 with tandem copies of the unmethylated chicken β-globin insulator region (CHB), which contains two functional CTCF binding sites and insulates *Igf2* in the paternal chromosome (Lee et al., 2010; Szabó et al., 2002; Figure 1C). Biallelic ICR1 insulation results in undetectable *Igf2* and in turn causes fetal growth retardation.

A double genetic rescue corrects growth anomalies of the BWS and SRS models

We predicted that a paternally inherited CHB allele rescues the overgrowth phenotype of the maternally inherited CTCFm allele. At the same time, a maternally inherited CTCFm allele should rescue the growth retardation of a paternally inherited CHB allele. We generated a rescue mouse model, CTCFm/CHB (Figure 1D), which is a compound heterozygote of the mutant alleles from the BWS model (CTCFm/+) and SRS model (+/CHB). We crossed +/CTCFm mothers with CHB/+ fathers to obtain offspring of four genotypes (Figures 1A–1D). We examined the resulting weanlings at 21 days postpartum (dpp), the newborns at 1 dpp, and fetuses at 18.5 days postcoitum (dpc) (Figures 1E–1G). We found three phenotypes and four genotypes: large (CTCFm/+), small (+/CHB), and normal (+/+ or CTCFm/CHB).

The mice of the rescue CTCFm/CHB genotype were indistinguishable from the wild-type siblings except by genotyping.

The weight of the CTCFm/+ and +/CHB weanlings was significantly larger and smaller than that of their +/+ siblings, respectively (Figure 2A). Importantly, the weight of the rescued CTCFm/CHB weanlings was statistically indistinguishable from the +/+ samples, indicating that the growth anomalies of both the BWS and SRS models were eliminated in the compound heterozygotes. We plotted the weight of the pups from birth until weaning age (Figure 2B). The CTCFm/+ pups were larger than their siblings and the +/CHB pups were smaller during postnatal growth. However, the weight of CTCFm/CHB pups remained indistinguishable from the +/+ pups during the first 3 weeks of life.

The weights of CTCFm/+ fetuses and placentas were significantly larger than those of their +/+ siblings at 18.5 dpc, whereas the +/CHB weights were significantly smaller than the weights of their +/+ siblings at 18.5 dpc (Figures 2C and 2D), which in agreement with our earlier work (Lee et al., 2010; Szabó et al., 2004). The size difference of +/CHB fetuses and placentas was already significantly different from the +/+ samples at 13.5 dpc. Importantly, the weights of the rescued CTCFm/CHB fetuses (Figure 2C) and placentas (Figure 2D) were statistically indistinguishable from those of +/+ samples at 13.5 dpc and at 18.5 dpc. Preliminary evidence suggested that the volume of the amniotic fluid may also differ in the CTCFm/+ versus +/+ and +/CHB/ versus +/+ genotypes but not between the CTCFm/CHB and +/+ genotypes.

To corroborate the results of this genetic rescue experiment, we generated CTCFm/CHB pups by crossing CTCFm/CTCFm females with CHB/+ males. The weights of the resulting CTCFm/CHB fetuses and placentas were significantly smaller than those of the CTCFm/+ fetuses at 18.5 dpc (Figure S2A), and the body weights remained smaller during postnatal growth (Figure S2B).

These results collectively support the hypothesis that the growth anomalies of the IGF2-dependent BWS model (at least the fetal overgrowth, placentomegaly, and macrosomia) and the growth anomalies of the IGF2-dependent SRS model (fetal growth retardation and microsomia) can be prevented by genetic rescue. It is important to note that the growth anomalies of both the BWS and SRS models were normalized in the compound heterozygotes already before birth and remained normalized after birth.

The genetic rescue corrects abnormal organ sizes in the BWS and SRS models

The overgrowth of different organs poses major problems in BWS children, and managing these complications is the major part of medical care in BWS patients after birth (Brioude et al., 2018). Congenital heart disease, including enlarged heart is found in 13%–20% of BWS cases, but the involvement of fetal IGF2 overexpression has not been recognized. Macroglossia is a common symptom in BWS children that often requires surgical reduction of the tongue. ICR1 gain of methylation (GOM) and paternal uniparental disomy (UPD), which both cause IGF2 overexpression, are risk factors for childhood tumors, such as in Wilms tumor of the kidney and hepatoblastoma of the liver (Brioude et al., 2019). We tested

whether the aberrant organ sizes can be corrected in the BWS and SRS models by genetically normalizing the ICR1 function.

We crossed +/CTCFm mothers with CHB/+ fathers and assessed the distribution of organ weight in the weaned pups. The brain weight was normal in the CTCFm/+ pups but was significantly smaller in the +/CHB pups than in +/+ pups (Figures 3A and 3B). The heart, kidney, liver, lung, and tongue organs were significantly larger in the CTCFm/+ than in the +/+ pups, whereas these organs were significantly smaller in the +/CHB than in the +/+ pups (Figures 3A and 3B). However, the weight of each organ of the CTCFm/CHB pups was indistinguishable from the +/+ pups (Figures 3A and 3B), except for the tongue that was slightly larger in the CTCFm/CHB pups.

We found that most of the internal organs were proportional to the body weight in both models, that is the relative organ/body weights of CTCFm/+ and +/CHB pups did not differ significantly from the +/+ pups, except for the brain and the tongue (Figure 3C; Figure S3). The brain/body ratio was slightly smaller in the CTCFm/+ pups and it was larger in the +/CHB pups than in the +/+ pups. This result is consistent with the relative microcephaly reported earlier of BWS (Lendvai et al., 1968) and relative macrocephaly of SRS (Wakeling et al., 2017) children. Relative microcephaly is no longer included in the description of BWS (Brioude et al., 2018), but because the BWS model had this phenotype, it was interesting to follow up on it. The relative brain weight of the CTCFm/CHB pups was indistinguishable from the +/+ pups (Figure 3C). The tongue/body ratio was significantly larger in CTCFm/+ than in +/+ pups. However, it was not significantly different between the CTCFm/CHB and +/+ pups. These results collectively demonstrate that the generalized organ weight anomalies found in the heart, kidney, liver, and lung of the BWS and SRS models can be corrected genetically by normalizing ICR1 insulation. In addition, the relative microcephaly and relative macrocephaly growth phenotypes of the IGF2-dependent BWS and SRS models, as well as the relative macroglossia of the BWS model, can also be corrected.

The double genetic rescue normalizes IGF2 levels at the fetal stage

We examined the underlying molecular mechanism of growth normalization in the compound heterozygous mice. Because both the CTCFm and CHB mutations misregulate the imprinted *Igf2* and *H19* genes, we expected that the misexpressions of these genes are the major cause of the body and organ size aberrations in the mutant genotypes. We collected 11 organs at 18.5 dpc and measured *Igf2* and *H19* transcript levels by using quantitative reverse-transcription PCR (Figures 4A and S4A) and quantified parental allele-specific transcription using multiplex allelotyping assays (Figures 4B and S4B). We found that the organ sizes at 21 dpp generally corresponded to the *Igf2* transcript levels at 18.5 dpc. The heart, kidney, liver, lung, and tongue organs were large, small, and normal-sized, respectively, in the CTCFm/+, +/CHB, and CTCFm/CHB weanlings (Figure 3A), and these organs exhibited 2-fold higher, greatly reduced, and normal *Igf2* RNA expression levels, respectively, at 18.5 dpc (Figure 4A). The liver was an exception, as its size was normalized in the rescue model at 21 dpp, but *Igf2* transcript levels were not normalized at 18.5 dpc (Figure 4A). Postnatal liver weight is, therefore, partially independent of fetal *Igf2* levels. The +/+ organs expressed *Igf2* from the paternal allele except the brain, which expressed

biallelic *Igf2* (Figure 4B), as expected (DeChiara et al., 1991). In agreement with the insulator model, elevated *Igf2* transcript levels in the CTCFm/+ fetus organs (Figure 4A) corresponded to biallelic *Igf2* transcription (Figure 4B). The brain of +/CHB pups was slightly but significantly smaller than normal (Figure 3A) and corresponded to reduced *Igf2* expression in the fetal brain (Figure 4A). The brain sizes were normal in the CTCFm/+ and CTCFm/CHB genotypes (Figure 3A), and *Igf2* expression levels were normal (Figure 4A). Relative microcephaly in the BWS model (Figure 3C) was consistent with the loss of imprinting of *Igf2* in the body only but not in the brain, where biallelic *Igf2* expression was unchanged (Figure 4B).

H19 transcript levels showed reciprocal patterns to *Igf2* transcript levels (Figure S4). For example, the CTCFm/+, +/CHB, and CTCFm/CHB organs had greatly reduced, 2-fold higher, and normal *H19* expression levels, respectively, compared to +/+ organs (Figure S4A). *H19* was maternally expressed in every +/+ fetal organ but was biallelically expressed in each organ of the +/CHB fetuses (Figure S4B). *H19* has no effect on body growth (Leighton et al., 1995a), whereas it slows the growth of the placenta immediately before birth (Keniry et al., 2012). A reduced or doubled level of *H19* (Figure S4A) may have contributed to the increased and reduced placenta size in the CTCFm/+ and +/CHB fetuses at 18.5 dpc (Figure 2D).

H19 and *Igf2* genes belong to an imprinted gene network (IGN), and *H19* long non-coding RNA (lncRNA) is a regulator of a large node of this IGN (Gabory et al., 2009; Monnier et al., 2013). To test whether the ICR1 affects allele-specific transcription beyond the *H19*/*Igf2* domain, we examined additional imprinted genes along distal chromosome 7 (Figure S5) and elsewhere (Figure S6). We found that, except for *H19*, *Igf2*, and *Igf2as*, the allele-specific expression of imprinted genes was undisturbed in the insulator mutants and in the compound heterozygotes. *Igf2as*, which is paternally expressed in the mouse (Moore et al., 1997), exhibited paternal expression in the +/+ organs except in the brain, where it was biallelic, and also showed biallelic expression in CTCFm/+ organs, similar to *Igf2* (Figure S5). These results (Figures S5 and S6) collectively suggest that the effects of the CTCFm or CHB mutations on allele-specific transcription are confined to the *H19/Igf2/Igf2as* imprinted domain along chromosome 7. This is reassuring for future gene therapy approaches that may target IGF2 or the ICR1 for *in utero* treatment of BWS and SRS cases.

We found, using western blotting, that the secreted IGF2 (IGF2s) peptide level was elevated 4-fold in the amniotic fluid of the BWS model and was close to undetectable in the SRS model at 13.5 dpc (Figure 4C). Importantly, the level of the IGF2 peptide was corrected to ~1-fold in the amniotic fluid of the compound heterozygous rescued fetuses. The level of the IGF2 precursor was also normalized in the amnion and the kidney. In summary, the BWS and SRS growth phenotypes were rescued in the CTCFm/CHB mice, which displayed corrected *Igf2* RNA and IGF2 protein levels (Figures 4A and 4C).

The IGF2-dependent BWS and SRS models are molecularly very similar to human BWS and SRS anomalies that predict IGF2 misexpressions (Figure S1); therefore, such human cases can be predicted to respond to the normalization of IGF2 levels or IGF2 signaling. Even though IGF2 has long been considered the culprit in both BWS and SRS, IGF2 is not

targeted in therapy. In human children, BWS and SRS are normally diagnosed and managed only after birth. Next, we present evidence in the mouse that the fetal stage is optimally suited for diagnosis and intervention in IGF2-dependent BWS and SRS because IGF2 activity is specific to the fetal stage.

The fetal stage presents a window of opportunity for diagnosing IGF2-dependent BWS and SRS growth aberrations

We measured *Igf2* transcript levels in the organs of the 18.5-dpc fetuses using quantitative reverse-transcription PCR (Figure 5A). We found that *Igf2* levels were much higher in the extraembryonic organs (placenta, yolk sac, and the amnion), than in the organs of the fetus body (liver, kidney, tongue, brain, heart, lung, muscle, and stomach). Among fetal organs, the liver exhibited the highest expression of *Igf2*, which plummeted after birth following a brief peak at 7 dpp and remained low during adulthood (Figure 5B). *Igf2* did not exhibit the brief postnatal surge in the kidney and brain. Postnatal downregulation of *Igf2* mRNA was also reported in the heart, muscle tongue, and lung (Weber et al., 2001; Constância et al., 2000; Lui et al., 2008). This expression pattern suggests that the IGF2 protein exerts its major growth-promoting effect during fetal development while the extraembryonic organs persist. It also implies that any intervention or diagnosis that targets IGF2 will be successful prenatally but not much longer after birth.

We found that the difference in fetus weights between CTCFm/+ samples and +/+ samples greatly increased between 16.5 dpc and 18.5 dpc (Figure 5C). The placenta weights were already 50% higher in CTCFm/+ samples than in the +/+ samples at 16.5 dpc (Figure 5D). These results show that the aberrant placenta growth in the IGF2-dependent BWS model at 16.5 dpc is indicative of the subsequent fetus overgrowth that occurs between 16.5 and 18.5 dpc. Thus, the late fetal stage represents a window of time when the IGF2-dependent BWS overgrowth may be intercepted.

IGF2 in the amniotic fluid is diagnostic of the SRS and BWS models

We performed western blotting using protein lysates from organs of a 13.5-dpc fetus and found that the full-length IGF2 protein, at ~18 kilodaltons (kDa), was clearly detectable in the amnion, yolk sac, and kidney; whereas the secreted IGF2 peptide (~8 kDa) was abundant only in the amniotic fluid (Figure 5E). Next, we explored the possibility of using IGF2 peptide level in the amniotic fluid as a fetal diagnostic marker in IGF2-dependent BWS and SRS. We found that the amniotic fluid had extremely low IGF2 peptide concentration in the SRS model (+/CHB) at 13.5 dpc (Figure 4C), at the time when the placenta weights indicated the SRS phenotype (Figure 2D). IGF2 peptide level was 4 times higher in the CTCFm/+ than in the +/+ amniotic fluid at 16.5 dpc (Figure 5F), when the placenta weights indicated the BWS phenotype (Figure 5D). These results show that IGF2 peptide levels in the amniotic fluid can be used as diagnostic targets in the SRS and BWS models at 13.5 and 16.5 dpc, respectively.

Pharmacological rescue of the BWS overgrowth phenotype

The results of the genetic rescue experiment were consistent with the idea that correcting IGF2 levels normalizes the growth anomalies in the BWS model. We next explored the

possibility of a pharmacological intervention in BWS. IGF2 signaling is mediated by the IGF1 receptor (IGF1R) (Baker et al., 1993; Bergman et al., 2013; Gicquel and Le Bouc, 2006). Picropodophyllin (PPP) is a drug approved by the Food and Drug Administration (FDA) to block IGF2 signaling. It is known to inhibit IGF1R kinase activity (Girnita et al., 2004). We treated CTCFm/+ and +/+ fetuses *in utero* with 20 mg/kg PPP for 2 days (starting on 16.5 dpc) or 5 days (starting on 13.5 dpc) and measured the weight of the fetuses and placentas at 18.5 dpc. We found a statistically significant reduction in the weight of PPP-treated CTCFm/+ fetuses (Figure 6A) compared with untreated CTCFm/+ controls after 2 days or 5 days of PPP treatment. The weight of CTCFm/+ fetuses was indistinguishable from that of +/+ control fetuses after 5 days of PPP treatment, suggesting that fetus weight was corrected in those mutants by PPP. The weight of +/+ fetuses was also significantly reduced after 2 days or 5 days of PPP but to a lesser extent than the CTCFm/+ fetuses. The weight of CTCFm/+ and +/+ placentas (Figure 6B) did not change significantly after 2 or 5 days of PPP, suggesting that contrary to what we found in the fetus, blocking the IGF1R does not reduce IGF2 activity in the placenta.

We also addressed the postnatal growth effects of PPP. The body weight of PPP-treated CTCFm/+ pups was significantly smaller than that of the untreated CTCFm/+ pups at the weaning age (Figure 6C) and was indistinguishable from the untreated +/+ pups, consistent with a rescued growth phenotype. Surprisingly, the weight of PPP-treated +/+ pups was not significantly smaller than the untreated +/+ pups (Figure 6C), suggesting that they can catch up in growth after the initial reduction at the fetal stage (Figure 6A). We then examined the organ weight at 21 dpp (Figure 6D). The PPP-treated CTCFm/+ heart was indistinguishable from the heart of the control +/+ pups, showing a complete rescue. The kidney and lung organs of the PPP-treated CTCFm/+ pups were significantly smaller than those of the CTCFm/+ control pups, although they were still slightly larger than those of the control +/+ pups, consistent with a partially rescued growth phenotype in those organs. The tongues of the PPP-treated and control CTCFm/+ pups were not significantly different. However, the difference between CTCFm/+ and +/+ tongues were highly significant ($p = 0.0002$), but the difference between PPP-treated CTCFm/+ and control +/+ tongues were hardly significant ($p = 0.048$), consistent with a partially rescued growth phenotype in the tongue as well (Figure 6D). PPP treatment did not result in reduced liver weight at weaning, and this may be related to the brief postnatal peak of *Igf2* transcription observed specifically in the liver (Figure 5B) or the independence of liver from IGF1R signaling. Because PPP affected the body weight but not the liver weight, the relative liver/body weights of CTCFm/+ and +/+ pups have increased after PPP (Figure 6E). The head/body (relative microcephaly) and tongue/body (relative macroglossia) phenotypes were corrected by the PPP intervention (Figure 6E). Importantly, none of the organs of PPP-treated +/+ pups changed significantly compared with the untreated controls. These results collectively suggest that most of the BWS-like overgrowth phenotypes can be intercepted by prenatal pharmacological intervention.

To confirm the mechanism of how PPP treatment rescues BWS overgrowth, we tested the effects of PPP on IGF1R signaling in the treated fetuses (Figure 6F). IGF2 binds to IGF1R and induces its autophosphorylation, which activates the Ras-mitogen-activated protein kinase (MAPK) and PI 3-kinase signaling pathways (Hakuno and Takahashi, 2018). In semi-

quantitative western blots, we found an increased level of phospho-IGF1R in the CTCFm/+ compared with that of the +/+ fetal kidneys at 18.5 dpc. The level of phospho-IGF1R was reduced in the PPP-treated CTCFm/+ samples compared with that of the control CTCFm/+ samples. In addition, we also found a reduction in phospho-MAPK (ERK1/2) and phospho-AKT in the PPP-treated samples compared with the control samples. These findings support the proposal that CTCFm/+ overgrowth in the kidney is mediated by the IGF2-IGF1R axis and that PPP corrects the overgrowth by interfering with IGF2 signaling.

We did not find any adverse effects of PPP treatment on the mothers. The animals were monitored daily, and no behavioral or physical abnormalities were observed during and after the treatment. All of the PPP-treated mothers nursed and groomed the pups until the weaning day. The weight gain of PPP-treated CTCFm/+ pregnant females was similar to that of the control mothers (Figure S7A), and they became pregnant again within the next 2 months. The number of fetuses was similar for the first (PPP-treated) and second (untreated) pregnancies of these females (Figure S7B). In summary, we demonstrated that the IGF2-dependent BWS fetal overgrowth phenotypes can be prevented by prenatal pharmacological intervention.

DISCUSSION

In this work, we presented evidence by using our IGF2-dependent BWS and SRS mouse models in support of IGF2-based *in utero* diagnosis and intervention strategies. We showed that (1) the prenatal intervention through genetically correcting IGF2 is successful in these models at the late stage of gestation, (2) a proof-of principle pharmacological method is available for normalizing IGF2 activity and fetal growth in the BWS model, (3) the placenta size anomalies are indicative of subsequent fetus growth anomalies in BWS and SRS, and (4) the secreted IGF2 peptide level in the amniotic fluid is a diagnostic biomarker for prenatal intervention. These results should encourage human studies in which BWS and SRS fetuses that exhibit IGF2 misexpressions are identified directly by measuring IGF2 peptide levels in the amniotic fluid and the IGF2 signaling output is adjusted *in utero* to normalize growth before birth.

What is realistic in prenatal management, in particular with respect to the window size between prenatal detection of SRS/BWS and successful prenatal treatment? The fetal stage is the optimal time for IGF2-based intervention because of the timing and the location of IGF2 expression. We found that the extraembryonic organs have the highest *Igf2* RNA and IGF2 protein levels, and these organs are only available at the fetal stage. We suggest that apart from the role of IGF2 in the placenta, the secreted IGF2 peptide supplied into the fluids surrounding the fetus by the amnion and yolk sac also has an important growth-promoting effect on the fetus. The majority of fetus growth takes place in the third trimester. Therefore, the last 3 months should be the most effective time window for intervention, considering that 5 days of PPP treatment was successful for correcting BWS overgrowth in the mouse.

Importantly, we suggest that the cases that would respond to IGF2 therapy could be identified by directly measuring IGF2 peptide levels. We found diagnostic 4-fold of normal

IGF2 peptide levels in the amniotic fluid of the BWS model at 16.5 pc and undetectable IGF2 in the SRS model at 13.5 dpc, before the fetuses showed abnormal growth (Figures 4 and 5). Based on these results in the mouse, we propose that human prenatal diagnosis could be done successfully by measuring IGF2 in the amniotic fluid. IGF2 was detected in human amniotic fluid and exocoelomic fluid by different methods (Blahovec et al., 2001; Chard et al., 1994; Merimee et al., 1984; Nonoshita et al., 1994). The exact IGF2 levels are contradictory in these studies due to the differences in the methodologies used for measuring IGF2 (Blahovec et al., 2001; Chard et al., 1994; Miell et al., 1997; Nonoshita et al., 1994), collecting amniotic fluid (Jauniaux and Gulbis, 2000), and statistics (Verhaeghe et al., 1999). These measurements will need to be revisited using uniform assays and should include verification by western blot.

Who should be screened for IGF2 level *in utero*? We suggest that every familial BWS and SRS pregnancy case should be screened for IGF2 peptide level. Other cases should be screened if indicated by anatomical and/or molecular defects characteristic of BWS and SRS that include ICR1 (Figure S1). Quantifying IGF2 levels in the amniotic fluid will reveal whether IGF2 levels are abnormal and also how much adjustment is necessary. We showed in the mouse that placenta size is an early indication of fetus size abnormalities in the BWS and SRS models. In a retrospective human study that included 12 BWS pregnancies, fetal ultrasound detected exomphalos, macroglossia, visceromegaly, polyhydramnios, and placentomegaly in 67%, 50%, 83%, 58%, and 83% of the cases, respectively, (Kagan et al., 2015). The median gestational age at the time of examination was 22.6 (range, 19.0–29.7) weeks. Aberrant IGF2 levels should be detected at these times according to the corresponding time points during mouse gestation (Figures 4 and 5). Children born by assisted reproductive technologies have a 4- to 10-fold increased frequency of BWS and SRS (Hiura et al., 2012; Mussa et al., 2017; Hattori et al., 2019), and a fraction of these children have a loss of methylation at ICR1. They may also benefit from IGF2 screening. We are optimistic that IGF2 detection will clearly identify the cases that can be helped by adjusting IGF2 signaling *in utero*.

Which cases would respond to *in utero* adjustment of IGF2 signaling? Based on the evidence in the mouse rescue models including the current work, we propose that IGF2-based intervention would be successful in each case that displays aberrant IGF2 levels, even though these may have very different molecular features (Figure S1). However, cases with normal IGF2 levels would not respond to IGF2 therapy even if they displayed specific molecular diagnostic features of BWS or SRS disorders, for example those positive for ICR2 epigenotype only. We predict that BWS cases with IGF2 overdose would respond to reducing the IGF2 signaling output and SRS cases with severely reduced IGF2 would benefit from IGF2 enhancing therapy *in utero*. We speculate that other imprinted disorders may respond to *in utero* IGF2 treatment if they displayed characteristic fetal growth anomalies and also diagnostic IGF2 levels. One possibility is Temple syndrome (TS14), which has overlapping symptoms with SRS, and TS14 fibroblasts with molecular abnormalities at 14q32.2 displayed low levels of *IGF2* RNA expression (Abi Habib et al., 2019).

Our results suggest successful strategies for normalizing IGF2 signaling *in utero*. IGF2 affects growth by signaling through IGF1R. A BWS case was recently reported with complex genetic abnormalities, paternal uniparental disomy of chromosome 11 (pat(11)dup), and 15q terminal deletion, resulting in two paternal *IGF2* copies and also *IGF1R* haploinsufficiency (Giabicani et al., 2019). The patient exhibited growth retardation after birth but not before birth. This finding is in agreement with the explanation that, as in the mouse, in humans the relative IGF2:IGF1R dose determines growth rate at the fetal stage but not postnatally. We showed that a specific inhibitor of IGF1R kinase activity, PPP (Girnita et al., 2004), reduced IGF2 signaling and normalized the growth in PPP-treated CTCFm/+ fetuses. Their body and internal organs were normal at the time of weaning, suggesting that the BWS-like overgrowth phenotype can be prevented pharmacologically by adjusting IGF2 signaling *in utero*. PPP affected the CTCFm/+ fetuses to a greater extent than the +/+ fetuses, perhaps because of the increased capacity of the larger CTCFm/+ placenta for transmitting PPP to the fetus. This result is reassuring for human intervention because twinning is relatively more common in BWS than in the general population (Weksberg et al., 2002; Cohen et al., 2019). Other drugs could also be considered, for example a number of different IGF1R targeting drugs that are FDA approved and/or are currently undergoing clinical trials for treating various diseases including cancer and thyroid eye disease (Dolgin, 2020). We have not rescued the SRS model's growth restriction phenotype pharmacologically, but such treatments are feasible based on large animal studies. IGF1 delivered into the amniotic fluid of intrauterine growth restriction model lambs increased the birth weight (Eremia et al., 2007; Spiroski et al., 2018). Similarly, fetal intra-amniotic IGF2 treatment would benefit human SRS cases that have severely reduced levels of IGF2. It is important to mention that the IGF2:IGF1 ratio is 12:1 in the human amniotic fluid (Merimee et al., 1984; Nonoshita et al., 1994).

We expect that as a consequence of correcting fetal growth and birth weight, other growth-dependent features can also be ameliorated or prevented by correcting IGF2 levels prenatally. We expect that the rescued newborns would continue to grow normally after birth, as we observed in the mouse rescue experiments. Among BWS symptoms, macroglossia would likely also respond to PPP based on our finding of the partially reduced tongue in weanlings that have undergone PPP treatment *in utero*. On the other hand, based on our results in the placenta (Figure 6B), we do not expect that placentomegaly could be prevented by PPP. This is consistent with genetic evidence suggesting that IGF1R is not responsible for IGF2 signaling in the placenta (Baker et al., 1993). This is perhaps less of a problem because the placenta is disposed at birth. The association between overgrowth and increased tumor risk in BWS is well documented (Brioude et al., 2019). Wilms tumor and hepatoblastoma display molecular defects consistent with IGF2 overexpression, such as loss of imprinting in the 11p15 region (Honda et al., 2008; Montagna et al., 1994; Rainier et al., 1995; Taniguchi et al., 1995). Overexpression of IGF2 was also detected in those tumors (Akmal et al., 1995; Scott et al., 1985). The tumor risk in BWS is the highest in patients with molecular defects that predict IGF2 overexpression (28% in patients with ICR1 GOM and 16% in patients with upd(11)pat) but low in patients with other molecular defects (2.6% in patients with ICR2 loss of methylation) (Maas et al., 2016; Mussa et al., 2016). We cannot directly address Wilms tumor and hepatoblastoma because these human complications are

not observed in the mouse BWS model. Our results (Figure 6D) predict that kidney size will be corrected in the child after correcting IGF2 signaling activity in the fetus, and this may result in a reduced Wilms tumor incidence. On the other hand, liver size may not be prevented by *in utero* PPP treatment (Figure 6D).

Pharmacological intervention for IGF2 could be continued postnatally in BWS children and may provide an additional benefit of reducing liver size considering that IGF2 has the longest postnatal presence in the liver. The major *IGF2* activity takes place before birth in human children as in the mouse (Constância et al., 2000; Weber et al., 2001; Lui et al., 2008; also see Figure 5), but the *IGF2* mRNA level has a brief postnatal peak at 2 months of age in humans, after which it declines to approximately one-tenth of the peak level (Li et al., 1996). The liver-specific promoter 1 (P1), specifically found in humans, is proposed as a major source of *IGF2* after birth (de Pagter-Holthuizen et al., 1988). We expect that an improvement in the BWS and SRS growth symptoms could be achieved by continuing IGF2-based therapies in the first year of life. However, if the correction takes place only after birth, these children will be born with a birth defect.

In summary, our results provide a proof-of-principle for clinical studies that will establish future prenatal diagnosis and treatment options of IGF2-dependent human BWS and SRS.

STAR★METHODS

RESOURCE AVAILABILITY

Lead contact—Further information and requests for resources and reagents should be directed to and will be fulfilled by the Lead Contact, Piroska E. Szabó (piroska.szabo@vai.org).

Materials availability—This study did not generate new unique reagents.

Data and code availability—The published article includes all datasets generated or analyzed during this study.

EXPERIMENTAL MODEL AND SUBJECT DETAILS

Mouse models—All animal experiments were performed according to the National Institutes of Health Guide for the Care and Use of Laboratory animals, with Institutional Care and Use Committee-approved protocols at Van Andel Institute (VAI). We previously generated the BWS and SRS models using gene targeting in 129SI/ImJ ES cells. The Pgkneo selection cassette was removed by crossing the mutant mice with the Hprt-Cre transgenic mouse line (Tang et al., 2002). The BWS model was created by introducing point mutations in the four CTCF binding sites (CTCFm) in the ICR1 allele (Szabó et al., 2004). To generate the SRS model we replaced the ICR1 with tandem copies of the unmethylated chicken β-globin insulator region (CHB), which contains two functional CTCF binding sites but due to mutagenesis it lacks the boundary elements of the chicken insulator (Lee et al., 2010). Genotyping primers are listed in Table S1. For the present study the CHB mutation was backcrossed ten times into JF1/MsJ inbred strain from The Jackson Laboratory (JAX 003720) to saturate the genome with SNPs, resulting in the CHB.JF1 sub line. Female and

male uterus-mate fetuses were used as biological replicates in the experiments that compare RNA levels, allelic expression, IGF2 protein levels or IGF2 signaling between the genotypes. Female and male embryos were combined from multiple pregnancies in experiments to plot growth between genotypes and between treated and control mice. Litter numbers, fetus, newborn, and weanling numbers are provided in the figure legends.

METHOD DETAILS

RNA isolation and quantification—We purified total RNA using RNA-Bee reagent (Tel-Test). To measure individual transcript levels, we prepared cDNA from 400 ng total RNA for qPCR assays as we did earlier (Lee et al., 2010). Contaminating DNA was removed with the DNA-free DNA Removal Kit (Ambion). Reverse transcription was performed using equal amount of RNA using the Superscript III Random Primer Synthesis kit (Invitrogen). The qRT-PCR primer sequences are listed in Table S2.

Sequenom allelotyping—To measure the portion of each parental allele in the total transcript levels we used a multiplex Sequenom (now Agena Bioscience) allelotyping assay as we did earlier (Iqbal et al., 2015). These assays are based on single nucleotide polymorphisms (SNPs) that distinguish between the inbred JF1/MsJ (JF1) and 129S1 (129) mouse strains. Each “unextended” primer (UEP) abuts a SNP in a target transcript, and the incorporating nucleotides differ in molecular mass between the parental alleles. The abundance of the extended UEP is quantified by mass spectrometry. Amplified cDNA samples were spotted onto a 384 SpectroCHIP Array (Agena Bioscience). Automated spectra acquisition was performed in a MassArrayCompact mass spectrometer (Sequenom) using the Spectroacquire program (Sequenom) and was analyzed by MassArray Typer v3.4. RNA-mixing standards were routinely run to verify linear response in measured versus input allele-specific transcription: for example, total RNA from JF1 and 129 embryos was mixed indifferent percent ratios (0:100, 10:90, 30:70, 50:50,70:30, 90:10, and 100:0) before cDNA preparation and Sequenom allelotyping. A 50:50 RNA mix was used for RNA skew correction. The percentage of transcription of each allele in the total expression was calculated at each given SNP. DNA samples were run from each embryo to verify the heterozygous genotype at each SNP. The unextended extend primer (UEP) and PCR primer sequences are listed in Table S3.

Western blot—We obtained amniotic fluid from 13.5 dpc and 16.5 dpc embryos by puncturing the visceral yolk sac and amnion and drawing about 50 μl liquid using a 19-gauge hypodermic needle attached to a 1 mL syringe. The maximum volume of amniotic fluid we harvested depended on the genotype: 50, 75, 75, and 110 μl was drawn from +/CHB, +/+, CTCFm/CHB, and CTCFm/+ genotypes at 13.5 dpc. We removed the cell content by centrifugation (in an Eppendorf centrifuge, 13000 rpm, 2 min at room temperature). We added equal volume of protein sample buffer (62.5 mM Tris, pH 6.8; 20% glycerol; 2% SDS; 5% 2-mercapto-ethanol; 0.05% Bromophenol Blue) according to the volume of the supernatant we collected. We boiled the sample for 10 minutes, and kept it frozen until electrophoresis. We also collected whole amnion in 50 μl protein sample buffer, whole yolk sac in 200 μl of protein sample buffer and one kidney in 50 μl of protein sample buffer. For detecting IGF2 at 13.5 dpc we used 3 μl of amniotic fluid, 2 μl of amnion, 0.5 μl

of yolk sac and 10 μl of kidney protein sample per well for electrophoresis in a 4%–20% gradient protein gel. After blotting, the membranes were incubated with an antibody against IGF2 (ABclonal Cat No A2086 1:1000). The signal was visualized by chemiluminescence and exposure to X-ray film. The images were scanned on a ChemiDoc XRS+ imaging system using Image Lab 5.2.1 (Bio-Rad) software and were quantified using the Fiji software.

For detecting IGF1R and its downstream targets we collected fetal kidney samples at 18.5 dpc. One kidney was homogenized in 200 μL of RIPA buffer supplemented with proteinase inhibitor and phosphatase inhibitors. The total lysate was left on ice for 30 minutes and sonicated for 5 minutes. After centrifugation for 15 minutes, the supernatant was transferred to a clean tube and the protein concentration was measured by spectroscopy at 280 nm. 10 μg protein was boiled with protein sample buffer and electrophoresed on a 4%–20% gradient SDS-polyacrylamide gel and blotted onto a PVDF membrane. Blots were first reacted with the anti-phosphorylated receptor antibody, then stripped and reacted with the pan-receptor antibody, then stripped again and reacted with the loading control anti-GAPDH antibody. The antibodies used for this experiment were IGF1 receptor (#3027), Phospho-IGF1 receptor (Tyr1135)(DA7A8) (#3918), AKT (C67E7) (#4691), Phospho-AKT (Ser473) (D9E)(#4060), p44/42 MAPK(Erk1/2)(137F5) (#4695), Phospho-p44/42 MAPK (Erk1/2) (Thr202/Tyr204)(D13.14.4E) (#4370). All six antibodies were from Cell Signaling Technology. The GAPDH antibody was from ABclonal (#AC035).

Treatment of mice with PPP—CTCFm/+ females were mated with +/+ males. They were orally dosed daily with 20 mg/kg PPP (AXL1717, APExBIO Cat No A3209) for two days starting at 16.5 dpc, or for five days, starting at 13.5 dpc using cheerio cereal (General Mills) as carrier. In a pilot experiment we used 40 mg/kg PPP for five days and observed a great reduction in the weight of fetuses, even below the untreated normal fetuses. Fetuses and placentas were collected on 18.5 dpc. To control for litter size and for a potential in utero competition between genotypes, we excluded from the analysis the small litters (less than 6 fetuses) and the litters that yielded only one genotype.

QUANTIFICATION AND STATISTICAL ANALYSIS

Statistical Methods—The normality of distribution within each group of samples was accessed using a Shapiro-Wilk test. If the *P*-value of the Shapiro-Wilk test was $p > 0.05$, then the data within the group was determined as normally distributed; whereas a $p < 0.05$ indicated that the data follow a non-normal distribution. For determining the significance between two normally distributed groups, a non-paired two-sided Student's t test was used to calculate *P*-values. When one or both groups followed non-normal distribution, a non-paired two-sided Wilcox rank sum test was performed to calculate *P*-values. Adjusted *P*-values between two or more normally distributed groups were determined by one-way ANOVA followed by a Tukey post hoc test. For multiple comparisons with at least one non-normally distributed group, Kruskal-Wallis was followed by Dunn's multiple comparison test to obtain Holm-Bonferroni adjusted *P* -values. Boxplots and statistics were generated using R v3.6.

Supplementary Material

Refer to Web version on PubMed Central for supplementary material.

ACKNOWLEDGMENTS

We thank Dr. Gerd Pfeifer (VAI) and Dr. Richard Leach (MSU) for helpful discussions, Dr. Timothy Geddes and Samreen Ahmed (Beaumont Hospital, Detroit) for performing the Sequenom allelotyping assays, and the Vivarium at VAI for mouse maintenance and husbandry. The assistance by Yanli Sun is greatly appreciated. This work was supported by R01 GM064378/GM/NIGMS NIH HHS/United States to P.E.S. and by VAI.

REFERENCES

Abi Habib W, Brioude F, Azzi S, Rossignol S, Linglart A, Sobrier ML, Giabicani É, Steunou V, Harbison MD, Le Bouc Y, and Netchine I (2019). Transcriptional profiling at the DLK1/MEG3 domain explains clinical overlap between imprinting disorders. Sci. Adv 5, eaau9425. [PubMed: 30801013]

Akmal SN, Yun K, MacLay J, Higami Y, and Ikeda T (1995). Insulin-like growth factor 2 and insulin-like growth factor binding protein 2 expression in hepatoblastoma. Hum. Pathol 26, 846–851. [PubMed: 7543440]

Azzi S, Abi Habib W, and Netchine I (2014). Beckwith-Wiedemann and Russell-Silver Syndromes: from new molecular insights to the comprehension of imprinting regulation. Curr. Opin. Endocrinol. Diabetes Obes 21, 30–38. [PubMed: 24322424]

Bachmann N, Crazzolara R, Bohne F, Kotzot D, Maurer K, Enklaar T, Prawitt D, and Bergmann C (2017). Novel deletion in 11p15.5 imprinting center region 1 in a patient with Beckwith-Wiedemann syndrome provides insight into distal enhancer regulation and tumorigenesis. Pediatr. Blood Cancer 64, 64. [PubMed: 27555087]

Baker J, Liu JP, Robertson EJ, and Efstratiadis A (1993). Role of insulin-like growth factors in embryonic and postnatal growth. Cell 75, 73–82. [PubMed: 8402902]

Bartolomei MS, Zemel S, and Tilghman SM (1991). Parental imprinting of the mouse H19 gene. Nature 351, 153–155. [PubMed: 1709450]

Begemann M, Zirn B, Santen G, Wirthgen E, Soellner L, Büttel HM, Schweizer R, van Workum W, Binder G, and Eggermann T (2015). Paternally Inherited IGF2 Mutation and Growth Restriction. N. Engl. J. Med 373, 349–356. [PubMed: 26154720]

Bell AC, and Felsenfeld G (2000). Methylation of a CTCF-dependent boundary controls imprinted expression of the Igf2 gene. Nature 405, 482–485. [PubMed: 10839546]

Bergman D, Halje M, Nordin M, and Engström W (2013). Insulin-like growth factor 2 in development and disease: a mini-review. Gerontology 59, 240–249. [PubMed: 23257688]

Binder G, Eggermann T, Weber K, Ferrand N, and Schweizer R (2017). The Diagnostic Value of IGF-2 and the IGF/IGFBP-3 System in Silver-Russell Syndrome. Horm. Res. Paediatr 88, 201–207. [PubMed: 28675902]

Blahovec J, Kostecka Z, Lacroix MC, Cabanié L, Godeau F, Mester J, and Cavaillé F (2001). Mitogenic activity of high molecular weight forms of insulin-like growth factor-II in amniotic fluid. J. Endocrinol 169, 563–572. [PubMed: 11375126]

Brioude F, Kalish JM, Mussa A, Foster AC, Bliek J, Ferrero GB, Boonen SE, Cole T, Baker R, Bertoletti M, et al. (2018). Expert consensus document: Clinical and molecular diagnosis, screening and management of Beckwith-Wiedemann syndrome: an international consensus statement. Nat. Rev. Endocrinol 14, 229–249. [PubMed: 29377879]

Brioude F, Toutain A, Giabicani E, Cottereau E, Cormier-Daire V, and Netchine I (2019). Overgrowth syndromes - clinical and molecular aspects and tumour risk. Nat. Rev. Endocrinol 15, 299–311. [PubMed: 30842651]

Chang S, and Bartolomei MS (2020). Modeling human epigenetic disorders in mice: Beckwith-Wiedemann syndrome and Silver-Russell syndrome. Dis. Model. Mech 13, dmm044123. [PubMed: 32424032]

Chard T, Blum WF, Brunjes J, Campbell DJ, and Wathen NC (1994). Levels of insulin-like growth factor-binding protein-2 and insulin-like growth factor-II in maternal serum, amniotic fluid and extraembryonic coelomic fluid at 9–20 weeks of pregnancy. J. Endocrinol 142, 379–383. [PubMed: 7523563]

Cohen JL, Duffy KA, Sajorda BJ, Hathaway ER, Gonzalez-Gandolfi CX, Richards-Yutz J, Gunter AT, Ganguly A, Kaplan J, Deardorff MA, and Kalish JM (2019). Diagnosis and management of the phenotypic spectrum of twins with Beckwith-Wiedemann syndrome. Am. J. Med. Genet. A 179, 1139–1147. [PubMed: 31067005]

Constância M, Dean W, Lopes S, Moore T, Kelsey G, and Reik W (2000). Deletion of a silencer element in Igf2 results in loss of imprinting independent of H19. Nat. Genet 26, 203–206. [PubMed: 11017078]

Constância M, Hemberger M, Hughes J, Dean W, Ferguson-Smith A, Fundele R, Stewart F, Kelsey G, Fowden A, Sibley C, and Reik W (2002). Placental-specific IGF-II is a major modulator of placental and fetal growth. Nature 417, 945–948. [PubMed: 12087403]

de Pagter-Holthuizen P, Jansen M, van der Kammen RA, van Schaik FM, and Sussenbach JS (1988). Differential expression of the human insulin-like growth factor II gene. Characterization of the IGF-II mRNAs and an mRNA encoding a putative IGF-II-associated protein. Biochim. Biophys. Acta 950, 282–295. [PubMed: 3167054]

DeChiara TM, Efstratiadis A, and Robertson EJ (1990). A growth-deficiency phenotype in heterozygous mice carrying an insulin-like growth factor II gene disrupted by targeting. Nature 345, 78–80. [PubMed: 2330056]

DeChiara TM, Robertson EJ, and Efstratiadis A (1991). Parental imprinting of the mouse insulin-like growth factor II gene. Cell 64, 849–859. [PubMed: 1997210]

Dolgin E (2020). IGF-1R drugs travel from cancer cradle to Graves'. Nat. Biotechnol 38, 385–388.

Eggenschwiler J, Ludwig T, Fisher P, Leighton PA, Tilghman SM, and Efstratiadis A (1997). Mouse mutant embryos overexpressing IGF-II exhibit phenotypic features of the Beckwith-Wiedemann and Simpson-Golabi-Behmel syndromes. Genes Dev. 11, 3128–3142. [PubMed: 9389646]

Eggermann T (2009). Silver-Russell and Beckwith-Wiedemann syndromes: opposite (epi)mutations in 11p15 result in opposite clinical pictures. Horm. Res 71, 30–35.

Eggermann T, Schönherr N, Meyer E, Obermann C, Mavany M, Eggermann K, Ranke MB, and Wollmann HA (2006). Epigenetic mutations in 11p15 in Silver-Russell syndrome are restricted to the telomeric imprinting domain. J. Med. Genet 43, 615–616. [PubMed: 16236811]

Engel N, West AG, Felsenfeld G, and Bartolomei MS (2004). Antagonism between DNA hypermethylation and enhancer-blocking activity at the H19 DMD is uncovered by CpG mutations. Nat. Genet 36, 883–888. [PubMed: 15273688]

Eremia SC, de Boo HA, Bloomfield FH, Oliver MH, and Harding JE (2007). Fetal and amniotic insulin-like growth factor-I supplements improve growth rate in intrauterine growth restriction fetal sheep. Endocrinology 148, 2963–2972. [PubMed: 17347307]

Ferguson-Smith AC, Sasaki H, Cattanach BM, and Surani MA (1993). Parental-origin-specific epigenetic modification of the mouse H19 gene. Nature 362, 751–755. [PubMed: 8469285]

Gabory A, Ripoche MA, Le Digarcher A, Watrin F, Ziyyat A, Forné T, Jammes H, Ainscough JF, Surani MA, Journot L, and Dandolo L (2009). H19 acts as a trans regulator of the imprinted gene network controlling growth in mice. Development 136, 3413–3421. [PubMed: 19762426]

Giabicani E, Chantot-Bastaraud S, Bonnard A, Rachid M, Whalen S, Netchine I, and Brioude F (2019). Roles of Type 1 Insulin-Like Growth Factor (IGF) Receptor and IGF-II in Growth Regulation: Evidence From a Patient Carrying Both an 11p Paternal Duplication and 15q Deletion. Front. Endocrinol. (Lausanne) 10, 263. [PubMed: 31114545]

Giannoukakis N, Deal C, Paquette J, Goodyer CG, and Polychronakos C (1993). Parental genomic imprinting of the human IGF2 gene. Nat. Genet 4, 98–101. [PubMed: 8099843]

Gicquel C, and Le Bouc Y (2006). Hormonal regulation of fetal growth. Horm. Res 65, 28–33.

Gicquel C, Rossignol S, Cabrol S, Houang M, Steunou V, Barbu V, Danton F, Thibaud N, Le Merrer M, Burglen L, et al. (2005). Epimutation of the telomeric imprinting center region on chromosome 11p15 in Silver-Russell syndrome. Nat. Genet 37, 1003–1007. [PubMed: 16086014]

Girnita A, Girnita L, del Prete F, Bartolazzi A, Larsson O, and Axelson M (2004). Cyclolignans as inhibitors of the insulin-like growth factor-1 receptor and malignant cell growth. Cancer Res. 64, 236–242. [PubMed: 14729630]

Hakuno F, and Takahashi SI (2018). IGF1 receptor signaling pathways. J. Mol. Endocrinol 61, T69–T86. [PubMed: 29535161]

Han L, Szabó PE, and Mann JR (2010). Postnatal survival of mice with maternal duplication of distal chromosome 7 induced by a Igf2/H19 imprinting control region lacking insulator function. PLoS Genet. 6, e1000803. [PubMed: 20062522]

Hark AT, Schoenherr CJ, Katz DJ, Ingram RS, Levorse JM, and Tilghman SM (2000). CTCF mediates methylation-sensitive enhancer-blocking activity at the H19/Igf2 locus. Nature 405, 486–489. [PubMed: 10839547]

Hattori H, Hiura H, Kitamura A, Miyauchi N, Kobayashi N, Takahashi S, Okae H, Kyono K, Kagami M, Ogata T, and Arima T (2019). Association of four imprinting disorders and ART. Clin. Epigenetics 11, 21. [PubMed: 30732658]

Hiura H, Okae H, Miyauchi N, Sato F, Sato A, Van De Pette M, John RM, Kagami M, Nakai K, Soejima H, et al. (2012). Characterization of DNA methylation errors in patients with imprinting disorders conceived by assisted reproduction technologies. Hum. Reprod 27, 2541–2548. [PubMed: 22674207]

Honda S, Arai Y, Haruta M, Sasaki F, Ohira M, Yamaoka H, Horie H, Nakagawara A, Hiyama E, Todo S, and Kaneko Y (2008). Loss of imprinting of IGF2 correlates with hypermethylation of the H19 differentially methylated region in hepatoblastoma. Br. J. Cancer 99, 1891–1899. [PubMed: 19034281]

Iqbal K, Tran DA, Li AX, Warden C, Bai AY, Singh P, Wu X, Pfeifer GP, and Szabó PE (2015). Deleterious effects of endocrine disruptors are corrected in the mammalian germline by epigenome reprogramming. Genome Biol. 16, 59. [PubMed: 25853433]

Jauniaux E, and Gulbis B (2000). Fluid compartments of the embryonic environment. Hum. Reprod. Update 6, 268–278. [PubMed: 10874572]

Kaffer CR, Srivastava M, Park KY, Ives E, Hsieh S, Batlle J, Grinberg A, Huang SP, and Pfeifer K (2000). A transcriptional insulator at the imprinted H19/Igf2 locus. Genes Dev. 14, 1908–1919. [PubMed: 10921905]

Kagan KO, Berg C, Dufke A, Geipel A, Hoopmann M, and Abele H (2015). Novel fetal and maternal sonographic findings in confirmed cases of Beckwith-Wiedemann syndrome. Prenat. Diagn 35, 394–399. [PubMed: 25641174]

Kalish JM, Jiang C, and Bartolomei MS (2014). Epigenetics and imprinting in human disease. Int. J. Dev. Biol 58, 291–298. [PubMed: 25023695]

Kanduri C, Pant V, Loukinov D, Pugacheva E, Qi CF, Wolffe A, Ohlsson R, and Lobanenkov VV (2000). Functional association of CTCF with the insulator upstream of the H19 gene is parent of origin-specific and methylation-sensitive. Curr. Biol 10, 853–856. [PubMed: 10899010]

Keniry A, Oxley D, Monnier P, Kyba M, Dandolo L, Smits G, and Reik W (2012). The H19 lincRNA is a developmental reservoir of miR-675 that suppresses growth and Igf1r. Nat. Cell Biol 14, 659–665. [PubMed: 22684254]

Lee DH, Singh P, Tsark WM, and Szabó PE (2010). Complete biallelic insulation at the H19/Igf2 imprinting control region position results in fetal growth retardation and perinatal lethality. PLoS One 5, e12630. [PubMed: 20838620]

Leighton PA, Ingram RS, Eggenschwiler J, Efstratiadis A, and Tilghman SM (1995a). Disruption of imprinting caused by deletion of the H19 gene region in mice. Nature 375, 34–39. [PubMed: 7536897]

Leighton PA, Saam JR, Ingram RS, Stewart CL, and Tilghman SM (1995b). An enhancer deletion affects both H19 and Igf2 expression. Genes Dev. 9, 2079–2089. [PubMed: 7544754]

Lendvai D, Cardi E, Ballati G, and Rezza E (1968). [Wiedemann-Beckwith syndrome. Description of a clinical case with macroglossia, umbilical hernia, hepatonephromegaly, relative microcephaly, macrosomy, and transient hypoglycemia]. Pediatria (Napoli) 76, 738–747. [PubMed: 5739619]

Li X, Cui H, Sandstedt B, Nordlinder H, Larsson E, and Ekström TJ (1996). Expression levels of the insulin-like growth factor-II gene (IGF2) in the human liver: developmental relationships of the four promoters. J. Endocrinol 149, 117–124. [PubMed: 8676043]

Liu D, Wang Y, Yang XA, and Liu D (2017). De Novo Mutation of Paternal IGF2 Gene Causing Silver-Russell Syndrome in a Sporadic Patient. Front. Genet 8, 105. [PubMed: 28848601]

Lui JC, Finkielstain GP, Barnes KM, and Baron J (2008). An imprinted gene network that controls mammalian somatic growth is down-regulated during postnatal growth deceleration in multiple organs. Am. J. Physiol. Regul. Integr. Comp. Physiol 295, R189–R196. [PubMed: 18448610]

Maas SM, Vansenne F, Kadouch DJ, Ibrahim A, Bliek J, Hopman S, Mannens MM, Merks JH, Maher ER, and Hennekam RC (2016). Phenotype, cancer risk, and surveillance in Beckwith-Wiedemann syndrome depending on molecular genetic subgroups. Am. J. Med. Genet. A 170, 2248–2260. [PubMed: 27419809]

McNeil DE, Langer JC, Choyke P, and DeBaun MR (2002). Feasibility of partial nephrectomy for Wilms' tumor in children with Beckwith-Wiedemann syndrome who have been screened with abdominal ultrasonography. J. Pediatr. Surg 37, 57–60. [PubMed: 11781987]

Merimee TJ, Grant M, and Tyson JE (1984). Insulin-like growth factors in amniotic fluid. J. Clin. Endocrinol. Metab 59, 752–755. [PubMed: 6384254]

Miell JP, Jauniaux E, Langford KS, Westwood M, White A, and Jones JS (1997). Insulin-like growth factor binding protein concentration and post-translational modification in embryological fluid. Mol. Hum. Reprod 3, 343–349. [PubMed: 9237262]

Monk D, Mackay DJG, Eggermann T, Maher ER, and Riccio A (2019). Genomic imprinting disorders: lessons on how genome, epigenome and environment interact. Nat. Rev. Genet 20, 235–248. [PubMed: 30647469]

Monnier P, Martinet C, Pontis J, Stancheva I, Ait-Si-Ali S, and Dandolo L (2013). H19 lncRNA controls gene expression of the Imprinted Gene Network by recruiting MBD1. Proc. Natl. Acad. Sci. USA 110, 20693–20698. [PubMed: 24297921]

Montagna M, Menin C, Chieco-Bianchi L, and D'Andrea E (1994). Occasional loss of constitutive heterozygosity at 11p15.5 and imprinting relaxation of the IGFII maternal allele in hepatoblastoma. J. Cancer Res. Clin. Oncol 120, 732–736. [PubMed: 7798299]

Moore T, Constancia M, Zubair M, Bailleul B, Feil R, Sasaki H, and Reik W (1997). Multiple imprinted sense and antisense transcripts, differential methylation and tandem repeats in a putative imprinting control region upstream of mouse Igf2. Proc. Natl. Acad. Sci. USA 94, 12509–12514. [PubMed: 9356480]

Mussa A, Molinatto C, Baldassarre G, Riberi E, Russo S, Larizza L, Riccio A, and Ferrero GB (2016). Cancer Risk in Beckwith-Wiedemann Syndrome: A Systematic Review and Meta-Analysis Outlining a Novel (Epi)Genotype Specific Histotype Targeted Screening Protocol. J. Pediatr 176, 142–149.e1. [PubMed: 27372391]

Mussa A, Molinatto C, Cerrato F, Palumbo O, Carella M, Baldassarre G, Carli D, Peris C, Riccio A, and Ferrero GB (2017). Assisted Reproductive Techniques and Risk of Beckwith-Wiedemann Syndrome. Pediatrics 140, e20164311. [PubMed: 28634246]

Naujokat H, Möller B, Terheyden H, Birkenfeld F, Caliebe D, Krause MF, Fischer-Brandies H, and Wiltfang J (2019). Tongue reduction in Beckwith-Wiedemann syndrome: outcome and treatment algorithm. Int. J. Oral Maxillofac. Surg 48, 9–16. [PubMed: 30057238]

Netchine I, Rossignol S, Azzi S, and Le Bouc Y (2013). Epigenetic anomalies in childhood growth disorders. Nestle Nutr. Inst. Workshop Ser 71, 65–73. [PubMed: 23502140]

Nonoshita LD, Wathen NC, Dsupin BA, Chard T, and Giudice LC (1994). Insulin-like growth factors (IGFs), IGF-binding proteins (IGFBPs), and proteolyzed IGFBP-3 in embryonic cavities in early human pregnancy: their potential relevance to maternal-embryonic and fetal interactions. J. Clin. Endocrinol. Metab 79, 1249–1255. [PubMed: 7525630]

Peñaherrera MS, Weindler S, Van Allen MI, Yong SL, Metzger DL, McGillivray B, Boerkoel C, Langlois S, and Robinson WP (2010). Methylation profiling in individuals with Russell-Silver syndrome. Am. J. Med. Genet. A 152A, 347–355. [PubMed: 20082469]

Rainier S, Dobry CJ, and Feinberg AP (1995). Loss of imprinting in hepatoblastoma. Cancer Res. 55, 1836–1838. [PubMed: 7728748]

Reik W, Brown KW, Schneid H, Le Bouc Y, Bickmore W, and Maher ER (1995). Imprinting mutations in the Beckwith-Wiedemann syndrome suggested by altered imprinting pattern in the IGF2-H19 domain. Hum. Mol. Genet 4, 2379–2385. [PubMed: 8634713]

Rentsendorj A, Mohan S, Szabó P, and Mann JR (2010). A genomic imprinting defect in mice traced to a single gene. Genetics 186, 917–927. [PubMed: 20713691]

Riccio A, Sparago A, Verde G, De Crescenzo A, Citro V, Cubellis MV, Ferrero GB, Silengo MC, Russo S, Larizza L, and Cerrato F (2009). Inherited and Sporadic Epimutations at the IGF2-H19 locus in Beckwith-Wiedemann syndrome and Wilms' tumor. Endocr. Dev 14, 1–9. [PubMed: 19293570]

Scott J, Cowell J, Robertson ME, Priestley LM, Wadey R, Hopkins B, Pritchard J, Bell GI, Rall LB, Graham CF, et al. (1985). Insulin-like growth factor-II gene expression in Wilms' tumour and embryonic tissues. Nature 317, 260–262. [PubMed: 2995818]

Singh P, Lee DH, and Szabó PE (2012). More than insulator: multiple roles of CTCF at the H19-Igf2 imprinted domain. Front. Genet 3, 214. [PubMed: 23087708]

Spiroski AM, Oliver MH, Jaquiery AL, Prickett TCR, Espiner EA, Harding JE, and Bloomfield FH (2018). Postnatal effects of intrauterine treatment of the growth-restricted ovine fetus with intra-amniotic insulin-like growth factor-1. J. Physiol 596, 5925–5945. [PubMed: 29235113]

Style CC, Cruz SM, Lau PE, Lee TC, Wesson DE, and Olutoye OO (2018). Surgical Outcomes of Patients with Beckwith-Wiedemann Syndrome. J. Pediatr. Surg 53, 1042–1045. [PubMed: 29551244]

Sun FL, Dean WL, Kelsey G, Allen ND, and Reik W (1997). Transactivation of Igf2 in a mouse model of Beckwith-Wiedemann syndrome. Nature 389, 809–815. [PubMed: 9349812]

Szabó P, Tang SH, Rentsendorj A, Pfeifer GP, and Mann JR (2000). Maternal-specific footprints at putative CTCF sites in the H19 imprinting control region give evidence for insulator function. Curr. Biol 10, 607–610. [PubMed: 10837224]

Szabó PE, Tang SH, Reed MR, Silva FJ, Tsark WM, and Mann JR (2002). The chicken beta-globin insulator element conveys chromatin boundary activity but not imprinting at the mouse Igf2/H19 domain. Development 129, 897–904. [PubMed: 11861473]

Szabó PE, Tang SH, Silva FJ, Tsark WM, and Mann JR (2004). Role of CTCF binding sites in the Igf2/H19 imprinting control region. Mol. Cell. Biol 24, 4791–4800. [PubMed: 15143173]

Tang SH, Silva FJ, Tsark WM, and Mann JR (2002). A Cre/loxP-deleter transgenic line in mouse strain 129S1/SvImJ. Genesis 32, 199–202. [PubMed: 11892008]

Taniguchi T, Sullivan MJ, Ogawa O, and Reeve AE (1995). Epigenetic changes encompassing the IGF2/H19 locus associated with relaxation of IGF2 imprinting and silencing of H19 in Wilms tumor. Proc. Natl. Acad. Sci. USA 92, 2159–2163. [PubMed: 7534414]

Thorvaldsen JL, Duran KL, and Bartolomei MS (1998). Deletion of the H19 differentially methylated domain results in loss of imprinted expression of H19 and Igf2. Genes Dev. 12, 3693–3702. [PubMed: 9851976]

Tunster SJ, Van de Pette M, and John RM (2011). Fetal overgrowth in the Cdkn1c mouse model of Beckwith-Wiedemann syndrome. Dis. Model. Mech 4, 814–821. [PubMed: 21729874]

Verhaeghe J, Coopmans W, van Herck E, van Schoubroeck D, Deprest JA, and Witters I (1999). IGF-I, IGF-II, IGF binding protein 1, and C-peptide in second trimester amniotic fluid are dependent on gestational age but do not predict weight at birth. Pediatr. Res 46, 101–108. [PubMed: 10400142]

Wakeling EL, Brioude F, Lokulo-Sodipe O, O'Connell SM, Salem J, Bliek J, Canton AP, Chrzanowska KH, Davies JH, Dias RP, et al. (2017). Diagnosis and management of Silver-Russell syndrome: first international consensus statement. Nat. Rev. Endocrinol 13, 105–124. [PubMed: 27585961]

Weber M, Milligan L, Delalbre A, Antoine E, Brunel C, Cathala G, and Forné T (2001). Extensive tissue-specific variation of allelic methylation in the Igf2 gene during mouse fetal development: relation to expression and imprinting. Mech. Dev 101, 133–141. [PubMed: 11231066]

Weksberg R, Shen DR, Fei YL, Song QL, and Squire J (1993). Disruption of insulin-like growth factor 2 imprinting in Beckwith-Wiedemann syndrome. Nat. Genet 5, 143–150. [PubMed: 8252039]

Weksberg R, Shuman C, Caluseriu O, Smith AC, Fei YL, Nishikawa J, Stockley TL, Best L, Chitayat D, Olney A, et al. (2002). Discordant KCNQ1OT1 imprinting in sets of monozygotic twins

discordant for Beckwith-Wiedemann syndrome. Hum. Mol. Genet 11, 1317–1325. [PubMed: 12019213]

Yamazawa K, Kagami M, Nagai T, Kondoh T, Onigata K, Maeyama K, Hasegawa T, Hasegawa Y, Yamazaki T, Mizuno S, et al. (2008). Molecular and clinical findings and their correlations in Silver-Russell syndrome: implications for a positive role of IGF2 in growth determination and differential imprinting regulation of the IGF2-H19 domain in bodies and placentas. J. Mol. Med. (Berl.) 86, 1171–1181. [PubMed: 18607558]

Yamoto K, Saitsu H, Nakagawa N, Nakajima H, Hasegawa T, Fujisawa Y, Kagami M, Fukami M, and Ogata T (2017). De novo IGF2 mutation on the paternal allele in a patient with Silver-Russell syndrome and ectrodactyly. Hum. Mutat 38, 953–958. [PubMed: 28489339]

Highlights

- Prenatal intervention is successful in BWS/SRS mouse models by targeting IGF2
- A pharmacological rescue is available to prenatally normalize IGF2 signaling in BWS
- Placenta growth indicates subsequent fetus growth anomalies in BWS/SRS models
- IGF2 peptide in the amniotic fluid is a diagnostic biomarker for BWS and SRS models

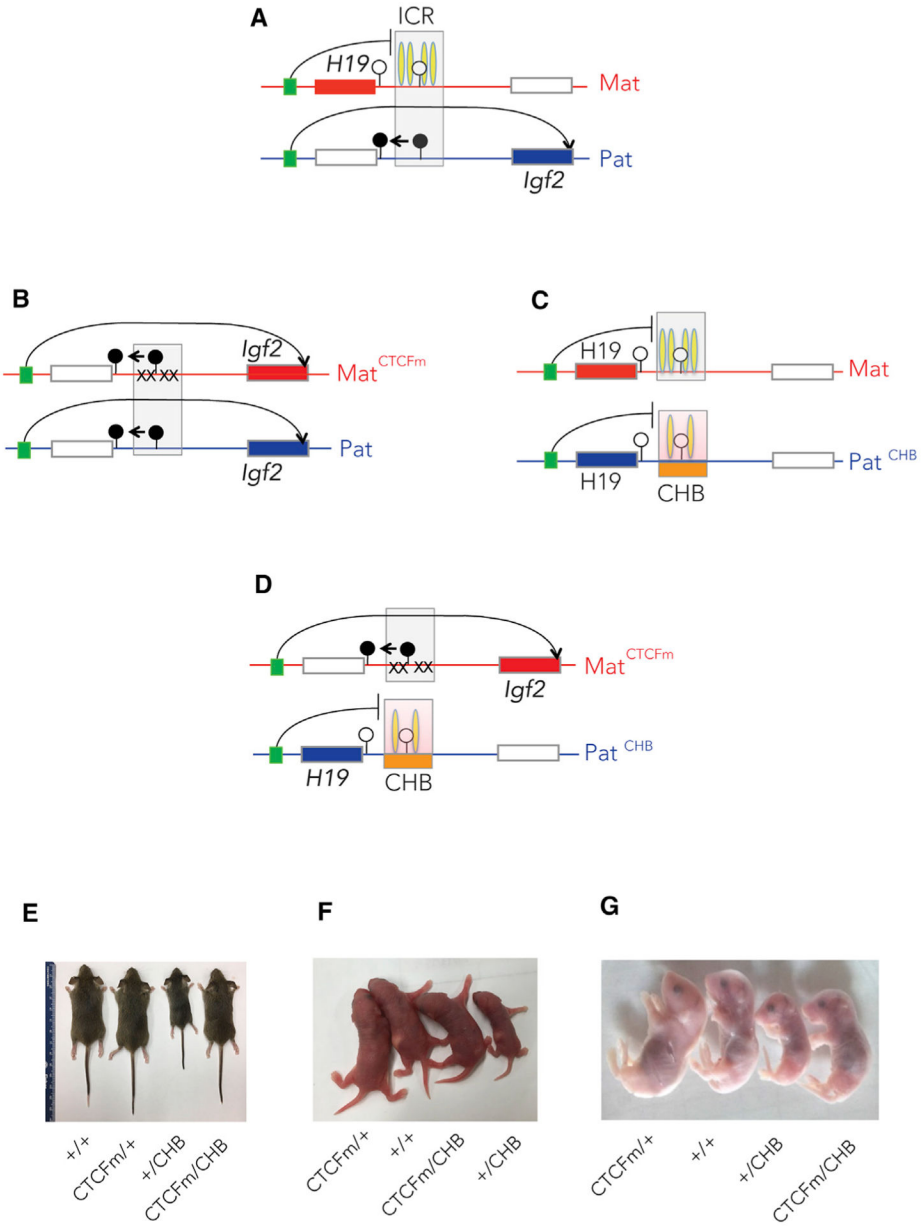

Figure 1. Mouse models for IGF2-dependent BWS and SRS

(A) The structure of the *H19/Igf2* domain is depicted in the normal +/+ mice. Imprinted genes expressed in the maternal and paternal chromosomes are shown as red and blue rectangles, respectively. CTCF insulator protein (yellow oval) binds the unmethylated maternal ICR1 allele, insulating the enhancers (green box) from the *Igf2* promoter. DNA methylation (black lollipops) in the paternal ICR1 prevents CTCF binding and thus allows *Igf2* promoter activation by the distant enhancers.

(B) BWS mouse model: CTCF binding is abolished by point mutations (x) in the maternal ICR1, resulting in biallelic *Igf2* expression.

(C) SRS mouse model: the paternal ICR1 is replaced by the mutant chicken beta globin insulator (CHB). The CHB is unmethylated, thus binds CTCF, and results in biallelic enhancer insulation and reduced *Igf2* expression.
(D) Rescue model: the compound heterozygote mice are expected to exhibit normalized ICR1 function and *Igf2* expression. To generate offspring with four genotypes, including the rescued one, +/CTCFm females were crossed with CHB/+ males.
(E) Representative weanling siblings are shown from the rescue cross, one genotype each at 21 days postpartum (dpp). Three phenotypes and four genotypes were recovered.
(F) Littermate newborn pups are shown from the rescue cross, one genotype each.
(G) Uterus-mate fetuses are shown from the rescue cross at 18.5 dpc.
See also Figure S1.

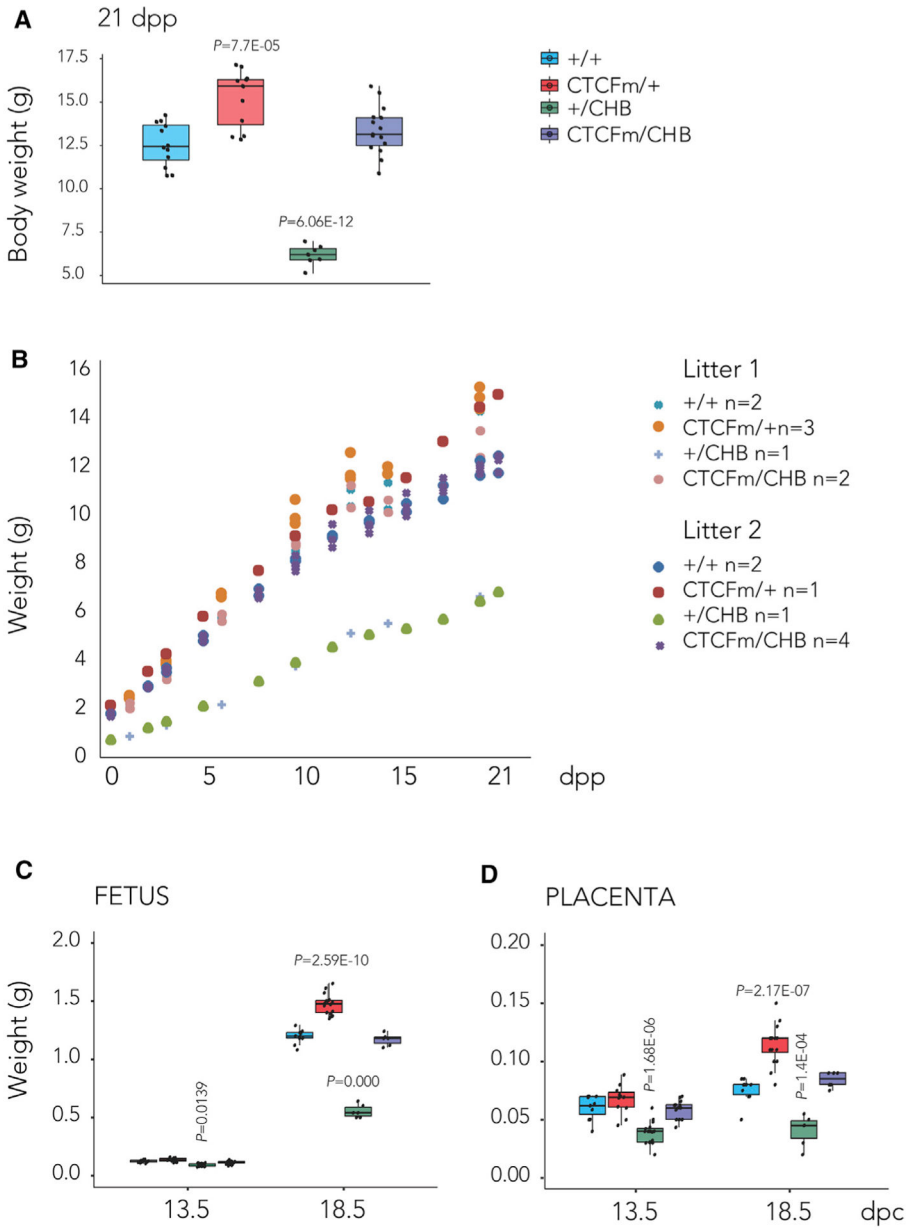

Figure 2. Genetic rescue corrects the growth phenotypes of BWS and SRS models

(A) Boxplot shows the weight distribution of pups on the day of weaning, +/+ (n = 12), CTCFm/+ (n = 14), +/CHB (n = 7), and CTCFm/CHB (n = 16). The data were collected from eight litters of +/CTCFm females crossed with CHB/+ males.

(B) Postnatal weight gain of individual pups from two litters is plotted by genotype from birth to weaning at 21 dpp.

(C and D) Boxplots depict the distribution of fetus (C) and placenta (D) weights for early (13.5 dpc) and late (18.5 dpc) fetal stages. The numbers of fetuses and placentas collected from multiple litters were as follows: +/+ (n = 11), CTCFm/+ (n = 11), +/CHB (n = 17), and CTCFm/CHB (n = 16) at 13.5 dpc; and +/+ (n = 10), CTCFm/+ (n = 16), +/CHB (n = 6),

and CTCFm/CHB (n = 6) at 18.5 dpc. The significant differences between mutant and +/+ samples are indicated.
See also Figure S2.

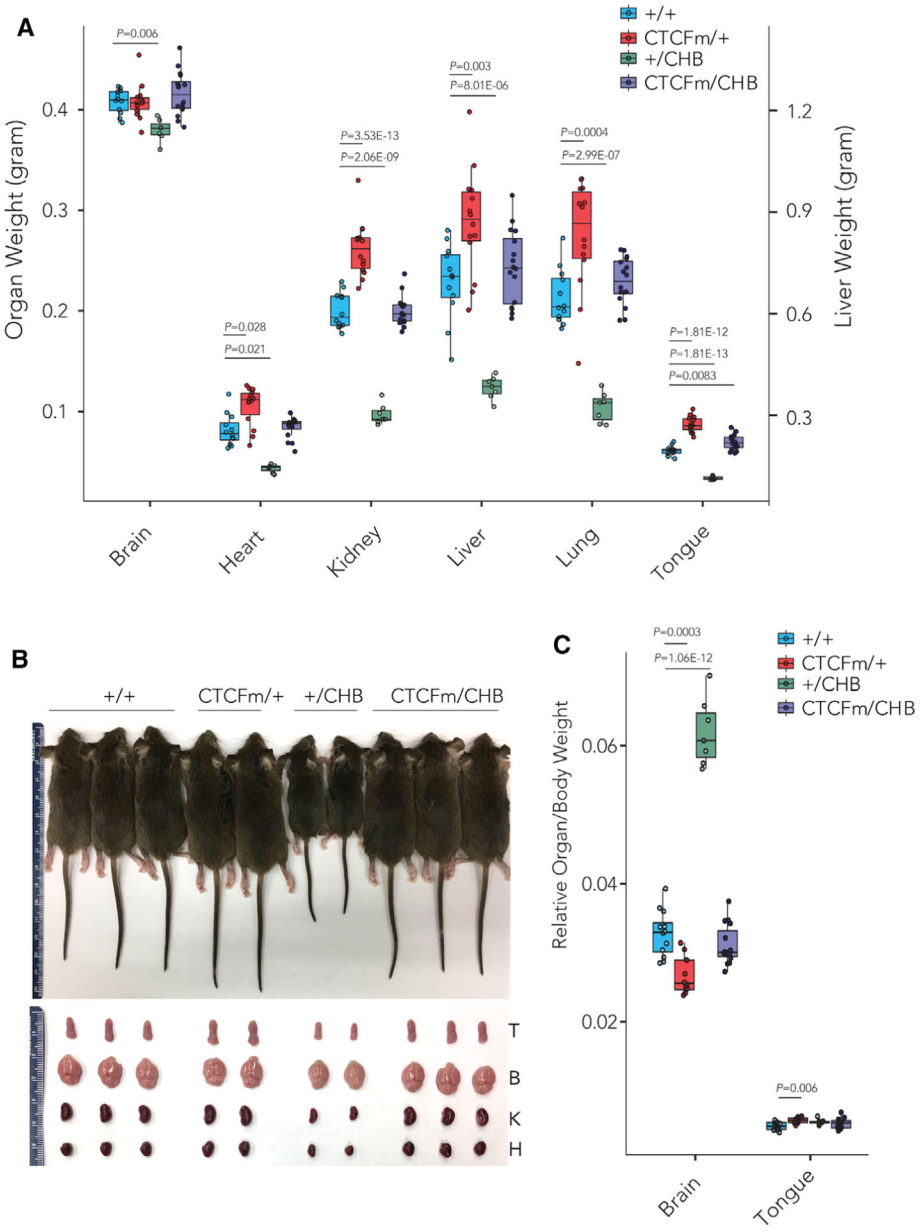

Figure 3. Organ weights are corrected in the compound heterozygote pups

(A) Boxplot shows the weight distribution of selected organs (or pairs of organs for lungs and kidneys) on the day of weaning. The liver values were plotted on a larger scale as shown to the right. The numbers of fetuses and placentas collected from multiple litters were +/+ (n = 11), CTCFm/+ (n = 11), +/CHB (n = 17), and CTCFm/CHB (n = 16) at 13.5 dpc; and +/+ (n = 10), CTCFm/+ (n = 16), +/CHB (n = 6), and CTCFm/CHB (n = 6) at 18.5 dpc. The significant differences between the different mutant genotypes compared to +/+ samples are marked with the p values.

(B) One litter of pups and some of their organs, namely, tongue (T), brain (B), kidney (K), and heart (H), are shown at weaning according to the genotypes indicated at the top.

(C) Boxplot shows the relative organ/body weights for the brain and the tongue. Other organs did not exhibit significant differences between mutant and +/+ genotypes.
See also Figure S3.

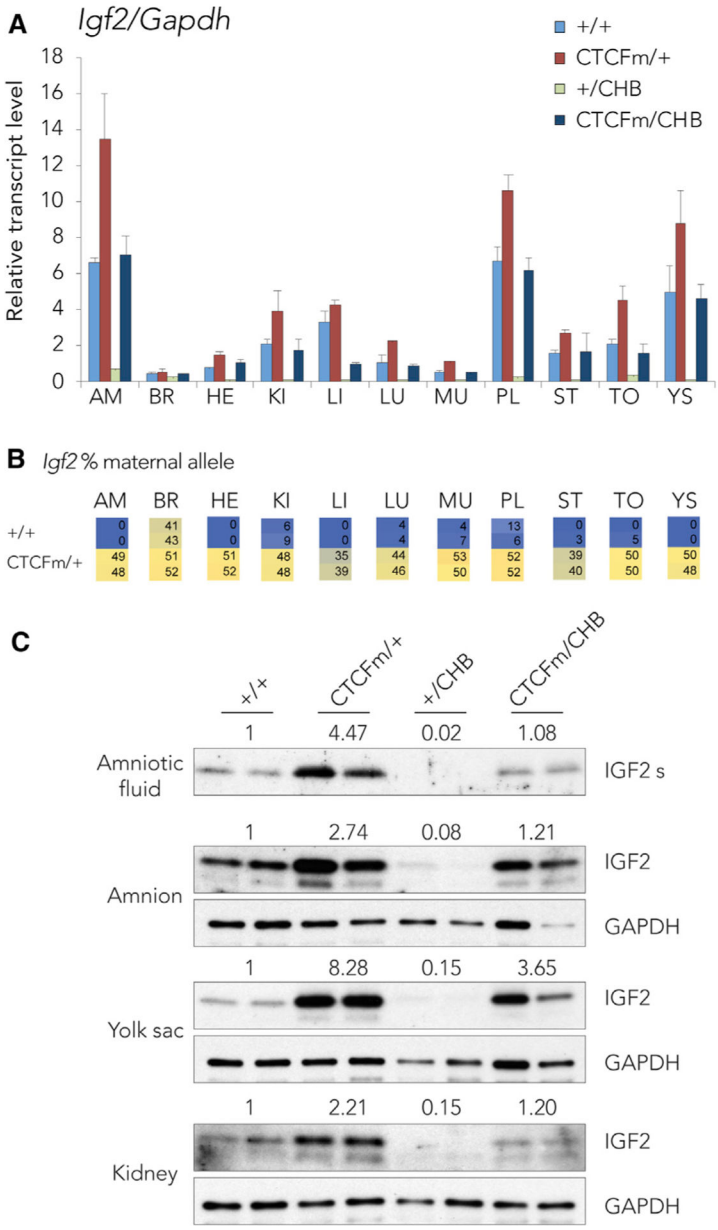

Figure 4. *Igf2* RNA and IGF2 protein levels are normalized in the genetically rescued fetuses

(A) Relative *Igf2/Gapdh* transcript levels are depicted in the major organs in the 18.5 dpc fetuses. Uterus-mate fetuses are shown, with one female and one male in each of the four genotypes as indicated by the color code. The average values of the biological duplicates are plotted with the standard deviation.

(B) Allele-specific expression of *Igf2* transcription in the major organs of the BWS model and normal 18.5-dpc fetuses. Uterus-mate fetuses are shown, with one female and one male in each genotype. The genotypes are shown to the left. The numbers refer to the percent maternal allele in the total expression determined using multiplex allelotyping assays. Single nucleotide polymorphisms between the 129S1 versus JF1/MsJ inbred mouse lines, inherited from the mothers and fathers, respectively, were used for quantifying parental alleles in the

Igf2 transcript. The colors depict paternal-allele-specific bias in blue and biallelic expression in yellow.

(C) IGF2 peptide levels are normalized in the rescued genotype. Western blot results are shown for the IGF2 signaling peptide (IGF2s) in the amniotic fluid and for the IGF2 protein in the amnion, yolk sac, and kidney organs of eight uterus-mate embryos, with one female and one male in each genotype, at 13.5 dpc. The four genotypes are marked at the top. The numbers above the images represent the relative average IGF2 protein values in the mutant compared with the +/+ samples after quantifying the film image by densitometry. Relative IGF2 levels were calculated between IGF2/GAPDH values except for the amniotic fluid. In the absence of cellular protein content, relative values were calculated based on IGF2 concentration per equal volumes of amniotic fluid in each sample.

For additional imprinted genes please see Figures S4, S5, and S6.

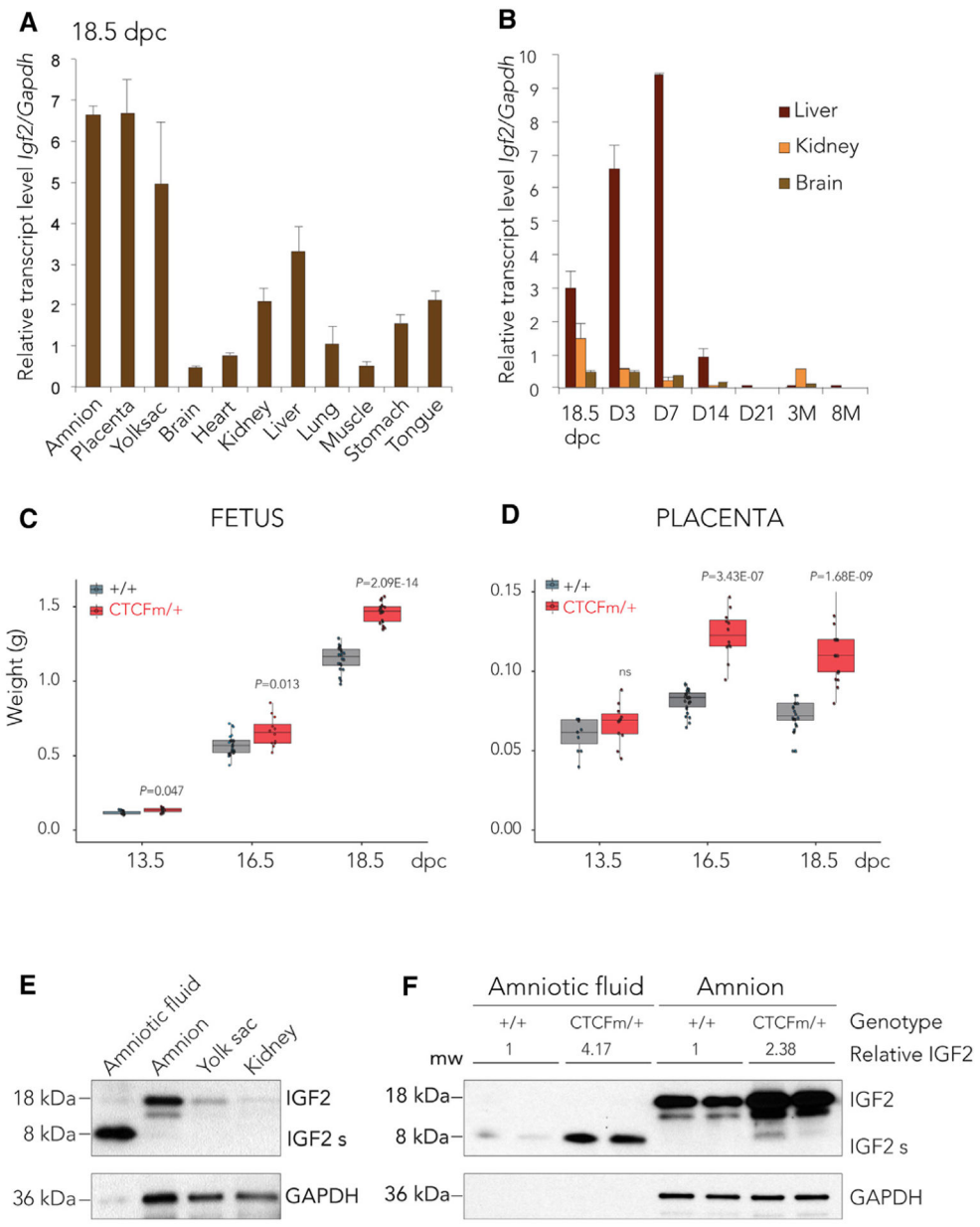

Figure 5. The fetal stage is best suited for intervention in IGF2-dependent BWS

(A) *Igf2* level is the highest in the extraembryonic organs of the fetus. Relative *Igf2/Gapdh* transcript levels are shown as detected by qRT-PCR in the extraembryonic and embryonic organs at 18.5 dpc using six biological replicates. The average values of replicate samples are plotted with the standard deviation.

(B) *Igf2* expression plummets soon after birth. Relative *Igf2/Gapdh* transcript levels are shown in the liver, kidney, and brain at 18.5 dpc, on postpartum day 3 (n = 2), day 7 (n = 2), day 14 (n = 3), day 21 (n = 4), 3 months (n = 1), and 8 months (n = 4); and in the kidney and brain on days 3, 7, and 14 and at 3 months (ns are as above).

(C and D) Abnormal placenta weight indicates subsequent BWS-like fetus weight anomaly. Growth curves in the BWS model. Fetus (C) and placenta (D) weights are depicted as

boxplots for early (13.5 dpc), mid (16.5 dpc), and late (18.5 dpc) fetal stages. The significance of differences between the CTCFm/+ and +/+ genotypes (p values, non-paired two-sided Student's t test) is marked. The numbers of fetuses and placentas were +/+ (n = 11) and CTCFm/+ (n = 11) at 13.5 dpc; +/+ (n = 24) and CTCFm/+ (n = 12) at 16.5 dpc; and +/+ (n = 20) and CTCFm/+ (n = 19) at 18.5 dpc. (E and F) IGF2 peptide level is diagnostic of BWS in the amniotic fluid. Western blots.

(E) The short, secreted IGF2 peptide (IGF2s) is detected in the amniotic fluid, and the full-length IGF2 protein is found in the organs at 13.5 dpc. GAPDH protein served as loading control.

(F) IGF2 levels are elevated in the amniotic fluid in the BWS model at 16.5 dpc. Uterus-mate samples, one female and one male, are shown from each genotype. The level of IGF2s and IGF2 protein was quantified in the amniotic fluid and in the amnion organ at 16.5 dpc by using densitometry of the film image. The numbers above the images represent relative average values of the CTCFm/+ compared with those of the +/+ samples.

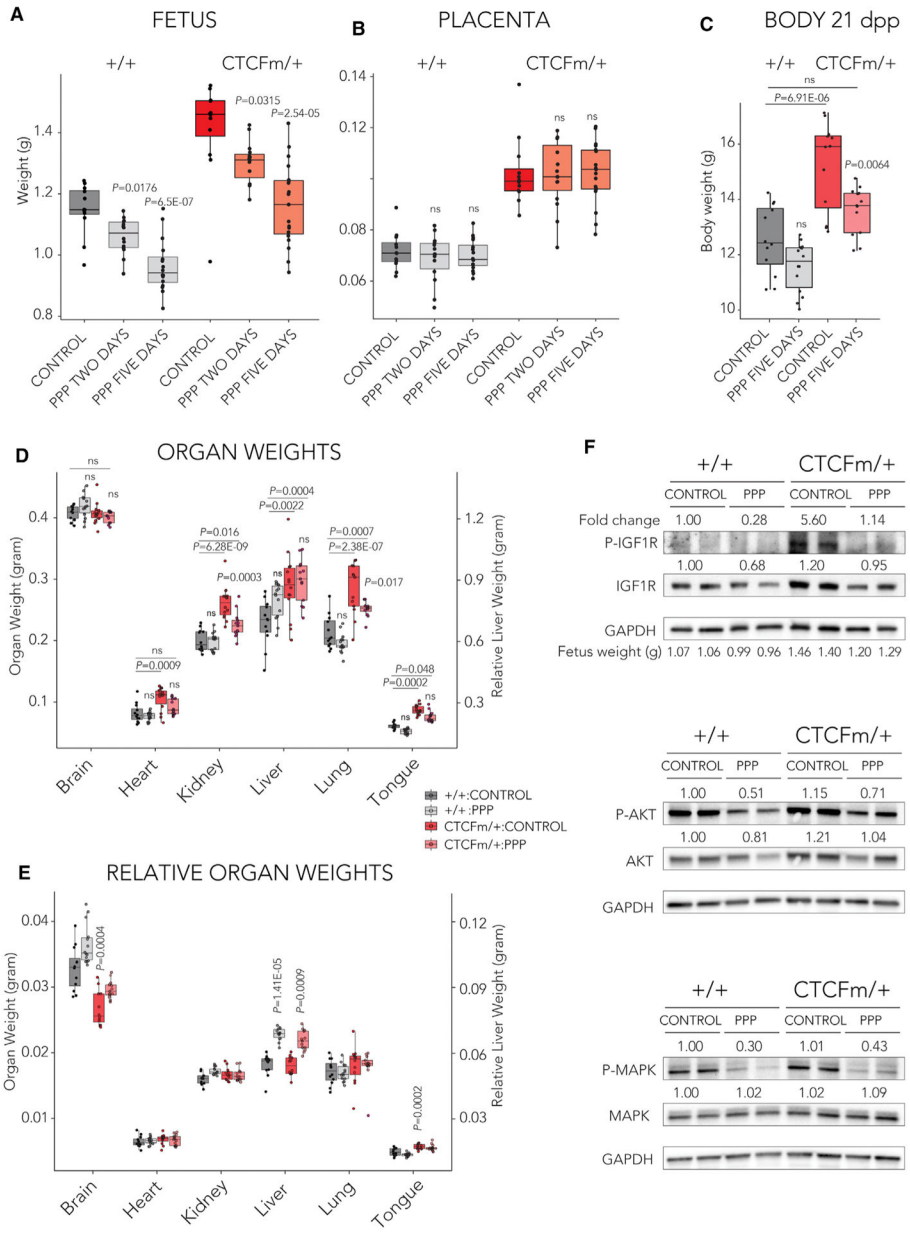

Figure 6. Prenatal pharmacological rescue of the BWS model

(A and B) Prenatal treatment by the IGF1R inhibitor picropodophyllin (PPP) antagonizes the IGF2 overdose and prevents fetal overgrowth in the BWS model fetuses. Boxplots show fetus (A) and placenta (B) weights from PPP-treated and control mothers. PPP was administered orally to CTCFm/+ pregnant dams at 20-mg/kg dose for 2 days, starting at 16.5 dpc CTCFm/+ (n = 15) and +/+ (n = 14), 4 litters, or for 5 days, starting at 13.5 dpc CTCFm/+ (n = 19) and +/+ (n = 16), 4 litters. Control fetuses CTCFm/+ (n = 12) and +/+ (n = 12) from 3 litters were untreated. Adjusted p values are shown to indicate the significant differences of treated versus control samples of the same genotype.

(C–E) Prenatal PPP prevents the overgrowth phenotypes of the weanling pups in the BWS model. Boxplots show the weight distribution of the total body (C), selected organ weights

(D), and relative organ/body weights (E) on the day of weaning at 21 dpp. The significant differences between treated CTCFm/+ and control +/+ samples and between treated CTCTm/CHB and control +/+ are marked above horizontal bars. The significance values between treated and control samples of the same genotype are indicated above the boxes. (F) PPP acts by blocking IGF1R signaling. Western blot of 18.5-dpc kidney samples. The protein lysates of two kidney samples, one female and one male, from each genotype and from each treatment group are displayed. Pan and phosphorylated IGF1R, AKT, and p44/42 MAPK(ERK1/2) antibodies were used. Fetus weights are provided at the bottom in the top panel. GAPDH was the loading control. The signals were quantified from the images, and averages of the duplicates are displayed as ratios of the altered conditions compared with the +/+ untreated samples.

See also Figure S7.

KEY RESOURCES TABLE

REAGENT or RESOURCE	SOURCE	IDENTIFIER
Antibodies		
IGF1 receptor	Cell Signaling Technology	Cat#3027; RRID:AB_2122378
Phospho-IGF1 receptor (Tyr1135)(DA7A8)	Cell Signaling Technology	Cat#3918; RRID:AB_10548764
AKT (C67E7)	Cell Signaling Technology	Cat#4691; RRID:AB_915783
Phospho-AKT (Ser473)(D9E)	Cell Signaling Technology	Cat#4060; RRID:AB_2315049
p44/42 MAPK(Erk1/2)(137F5)	Cell Signaling Technology	Cat#4695; RRID:AB_390779
Phospho-p44/42 MAPK (Erk1/2)(Thr202/Tyr204)(D13.14.4E)	Cell Signaling Technology	Cat#4370; RRID:AB_2315112
GAPDH antibody	ABclonal	Cat#AC035; RRID:AB_2769863
IGF2 antibody	ABclonal	Cat#A2086; RRID:AB_2764106
Chemicals, peptides, and recombinant proteins		
PPP (AXL1717)	APExBIO	Cat#A3209
Critical commercial assays		
RNA-Bee reagent	Tel-Test	Cat#CS-104B
Superscript III Random Primer Synthesis kit (Invitrogen™)	ThermoFisher Scientific	Cat#18080051
DNA-free™ DNA Removal Kit (Ambion™)	ThermoFisher Scientific	Cat#AM1906
384 SpectroCHIP Array	Agena Bioscience	Cat#10411
Experimental models: organisms/strains		
Mouse: $Rr27^{tm1Pes}$ (CTCFm)	Szabó et al., 2004	RRID:MGI:3046755
Mouse: $Rr27^{tm4Pes}$ (CHB)	Lee et al., 2010	N/A
JF1/MsJ inbred strain	The Jackson Laboratory	JAX: 003720; RRID:IMSR_JAX:003720
Oligonucleotides		
Primers for genotyping, see Table S1	This paper and Lee et al., 2010	N/A
Primers for RT-PCR, see Table S2	Lee et al., 2010	N/A
Primers for Sequenom allelotyping, see Table S3	This paper	N/A
Software and algorithms		
SpectroAcquire	Agena (formerly Sequenom)	N/A
MassArray Typer v3.4	Agena (formerly Sequenom)	N/A